M V M   Mobility Vehicle Mechanics

THE SAFETY ISSUES OF HYDROGEN-GASOLINE DUAL-FUEL INJECTION IN NATURAL ASPIRATED INTERNAL COMBUSTION ENGINES

Attila Kiss[1], Bálint Szabó[2], Zoltán Weltsch[3]

ABSTRACT: Hydrogen-gasoline dual-fuelled internal combustion engines (ICEs) have emerged as a viable alternative to conventional gasoline engines, promising reduced emissions and improved fuel efficiency. The integration of hydrogen as a supplementary fuel in naturally aspirated engines, however, introduces a critical challenge that affects engine performance. Nevertheless, it also introduces significant security challenges, notably the increased risk of backfire within the intake manifold. This study investigates the security issues associated with hydrogen-gasoline dual-fuel engines, with a particular focus on the propensity for intake manifold backfire due to the presence of hydrogen. Through experimental analysis and simulations, the study explores various techniques to eliminate or reduce the occurrence of backfire. These techniques include optimized fuel injection timing and camshaft modification. The results of the simulation show how the modifications affect the basic characteristics of the natural aspirated internal combustion engine.

[1] *Attila Kiss, John von Neumann University, 6000 Kecskemét Izsáki Street 10, Hungary, kiss.attila@nje.hu, -*(Corresponding author)*
[2] *Bálint Szabó, BDN Automotive Kft., 9025 Győr, Kereszt Street 3-5, Hungary, balint.szabo@bdn-automotive.com, -*
[3] *Dr. Zoltán Weltsch, Széchenyi Istvan University, 9026 Győr Egyetem Square 1, Hungary, weltsch.zoltan@sze.hu, -*

PITANJA SIGURNOSTI UBRIZGAVANJA DUALNOG GORIVA VODONIK-BENZIN GORIVA U ATMOSFERSKE MOTORE

REZIME: Motori sa unutrašnjim sagorevanj em (ICE) sa dualnim gorivom vodonik-benzin su se pojavili kao održiva alternativa konvencionalnim benzinskim motorima, obećavajući smanjene emisije i poboljšanu efikasnost sagorevanja. Međutim, integracija vodonika kao dodatnog goriva u atmosferskim motorima predstavlja kritičan izazov koji utiče na performanse motora. Ipak, on takođe uvodi značajne bezbednosne izazove, posebno povećan rizik od povratnog udara unutar usisne grane. Ova studija istražuje bezbednosna pitanja povezana sa vodonik-benzinskim motorima sa dualnim gorivom, sa posebnim fokusom na sklonost povratnom udaru usisne grane usled prisustva vodonika. Kroz eksperimentalnu analizu i simulacije, studija istražuje različite tehnike za eliminisanje ili smanjenje pojave povratnog udara. Ove tehnike uključuju optimizovano vreme ubrizgavanja goriva i modifikaciju bregastog vratila. Rezultati simulacije pokazuju kako modifikacije utiču na osnovne karakteristike atmosferskog motora sa unutrašnjim sagorevanjem.

KLJUČNE REČI: *vodonik, dualno gorivo, formiranje hibridne mešavine*

THE SAFETY ISSUES OF HYDROGEN-GASOLINE DUAL-FUEL INJECTION IN NATURAL ASPIRATED INTERNAL COMBUSTION ENGINES

Attila Kiss, Bálint Szabó, Zoltán Weltsch

INTRODUCTION

The growing concerns over environmental pollution and the depletion of fossil fuels have accelerated the search for cleaner and more efficient energy sources. Hydrogen has emerged as a promising alternative due to its high energy density and zero carbon emissions when combusted. Its potential as a sustainable fuel has been extensively reviewed, highlighting the challenges associated with its production, storage, and transportation Abdalla et al. [1]. One of the most viable applications of hydrogen is its use in internal combustion engines (ICEs), either as a standalone fuel or in combination with conventional fuels such as gasoline.

Hydrogen-gasoline dual-fuel engines offer a practical solution for reducing emissions while maintaining the operational flexibility of traditional ICEs. This approach leverages the existing infrastructure and engine technologies, making it a transitional strategy towards cleaner automotive solutions. However, integrating hydrogen into ICEs presents several challenges, such as backfire, pre-ignition, and knock, due to hydrogen's high reactivity and low ignition energy Aghahasani et al. [2]. Furthermore, the precise control of the air-fuel mixture and combustion timing is crucial to ensure stable engine operation and to optimize performance and emissions.

Recent studies have explored various strategies to enhance the performance and emissions characteristics of hydrogen-gasoline dual-fuel engines. For instance, Aghahasani et al. [2] conducted a numerical study on hydrogen-gasoline dual-fuel spark ignition engines, demonstrating that the addition of hydrogen can significantly improve thermal efficiency and reduce CO_2 emissions. However, this improvement often comes at the cost of increased nitrogen oxide (NOx) emissions due to higher in-cylinder temperatures. Similarly, Akal et al. [3] emphasized the need for advanced engine control techniques, such as water injection and multi-objective optimization, to balance performance and emissions in dual-fuel configurations.

The addition of hydrogen to gasoline engines has been shown to enhance flame speed and combustion stability, leading to improved engine efficiency D'Andrea et al. [4]. However, optimizing hydrogen use in ICE's requires careful management of fuel injection timing and mixture formation. Salek et al. [5] demonstrated the benefits of port water injection in reducing NOx emissions in a hydrogen-gasoline dual-fuel engine, highlighting the potential of advanced control strategies to mitigate the adverse effects of hydrogen combustion.

This study builds on the existing body of research by investigating a novel approach to optimize the performance and emissions of a hydrogen-gasoline dual-fuel engine. We propose a modification to the camshaft profile that delays the intake valve closure, reducing the risk of backfire and improving combustion stability. This modification is designed to limit the intake of hydrogen during critical phases of the intake stroke, thereby preventing premature ignition and enhancing engine reliability.

The remainder of this paper presents the experimental setup and methodology used to evaluate the impact of the camshaft modification on engine performance and emissions. The results are compared with existing studies, providing insights into the trade-offs between

power output, fuel efficiency, and emissions. By addressing the challenges associated with hydrogen integration in ICE's, this research contributes to the development of more efficient and environmentally friendly automotive technologies, enhancing overall engine stability. While similar approaches have been explored in recent studies, our work offers a more refined camshaft design tailored for dual-fuel applications.

Despite the benefits in backfire prevention and emissions reduction, the delayed intake valve closure introduces some trade-offs. The modification leads to a reduction in engine power output and torque, as the shortened intake phase limits the air-fuel mixture entering the cylinder. Nonetheless, the environmental advantages, such as reduced nitrogen oxides (NO_x) emissions and improved combustion stability, outweigh the performance drawbacks, making this approach viable for eco-friendly applications.

1   MATERIALS AND METHODS

1.1   Engine

For the test series, we used a gasoline-powered M42B18 internal combustion engine produced by BMW, which was completely renovated before the research. The basic parameters of the engine are listed in ***Table 1***.

Table 1 Engine parameters [7]

Engine code	M43B18
Stroke	Four strokes
Layout	Inline-4
Fuel type	Gasoline
Displacement	1796 [cm^3]
Fuel system	Manifold injection
Firing order	1-3-4-2
Compression ration	9.7:1
Cylinder bore	84 [mm]
Piston stroke	81 [mm]
Valve arrangement	SOHC
Valves number	8, 2 valves per cylinder
Camshaft Total duration (intake)	244°
Camshaft total duration (exhaust)	244°
Intake valves maximum lift	10 [mm]
Exhaust valves masimum lift	10 [mm]
Valves overlap	35°

In order to avoid backburn, the profile of the original camshaft was modified in such a way that no valve lock occurs, and in fact, 9 degrees pass without any of the valves being open. Thanks to this, it cannot happen that the hot exhaust gas ignites the mixture of hydrogen, gasoline and air left in the intake pipe. ***Table 2*** contains the data of the modified camshaft.

Table 2 Modified camshaft parameters

Camshaft Total duration (intake)	200°
Camshaft total duration (exhaust)	200°
Intake valves maximum lift	8,5 [mm]
Exhaust valves masimum lift	8,5 [mm]
Valves overlap	-9°

1.2 Simulation

1.2.1 Structure of the simulation

A 1D simulation model of the engine was developed using AVL Cruise-M to simulate gas exchange, performance, and emissions. The software enables the construction of a complex engine model by utilizing built-in modules such as cylinders, pipes, junctions, throttles, and injectors. As a result, the intake and exhaust systems of the engine must be modelled with high accuracy, including the valve lift curves and the flow coefficients of the cylinder head ports and valves. The basic geometric parameters of the engine, as previously described, were used in this model. In our previous research, we validated the purely gasoline-powered simulation in a brake bench environment. This measurement took place as follows. The validation measurements were conducted across a range of engine speeds from 1000 to 4500 rpm, starting at 500 rpm, using gasoline as the fuel. To optimize engine efficiency, power, and emissions, lambda was maintained at 1, ensuring a stoichiometric air-fuel mixture. Additionally, the maximum possible spark timing was set just below the knock threshold before top dead centre (TDC), with the throttle body fully open. These conditions were chosen to achieve the highest performance at each measurement point by minimizing losses through the throttle valve, allowing for future comparisons of power output and emissions that are solely influenced by changes in fuel type.

Friction calculations were performed using the built-in Patton, Nitschke, Heywood model [6], while the heat release was defined using the Vibe 2-zone model to align with the combustion parameters measured on the actual engine. The following section presents the combustion parameters:
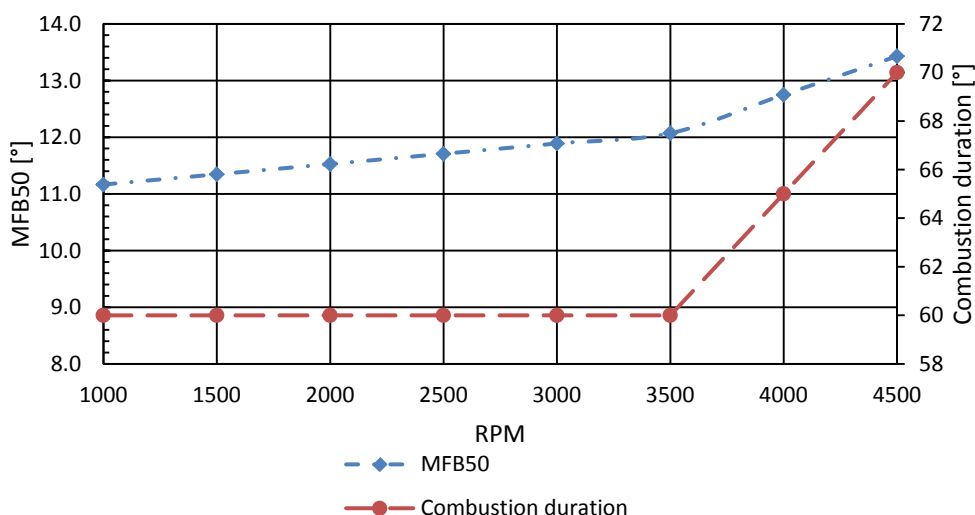
Figure 1. Combustion parameters

The parameters "m" and "a" were set to 6.9 and 1.9, respectively, for all engine speeds. The engine is connected to ambient boundaries on both the intake and exhaust sides, with temperature and pressure maintained at steady-state ambient values.

The valve lift curves were measured directly on the actual cylinder head with a crank angle resolution of 4° for both the intake and exhaust sides.
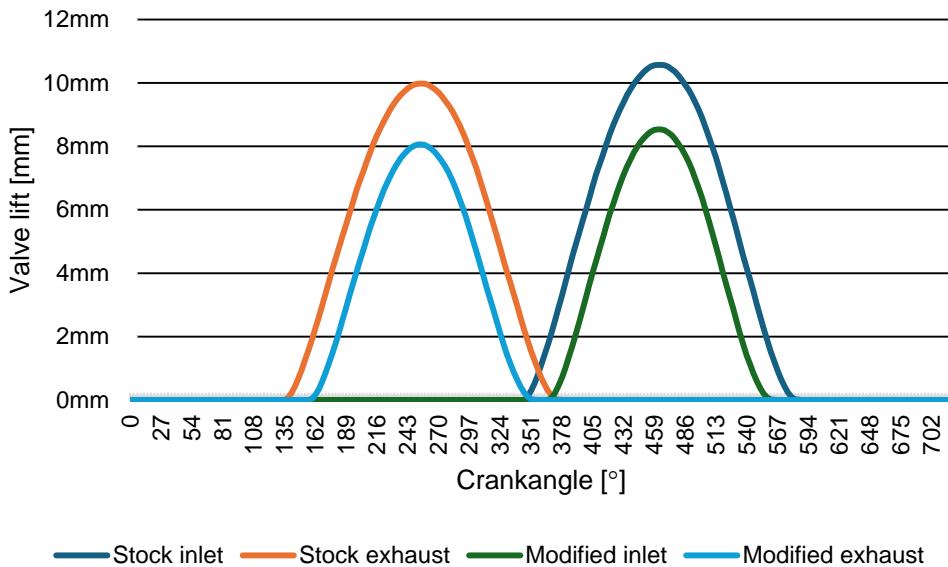
Figure 2. Valve lift curve (original and modified)

The valve lift curves of both the original and modified camshaft designs are illustrated in the Figure 2. The comparison between the two profiles reveals significant differences in valve operation characteristics. For the original camshaft, the typical valve lift pattern shows a standard opening and closing sequence, allowing for optimal airflow into and out of the cylinder during the intake and exhaust strokes. This configuration is designed to maximize the engine's volumetric efficiency and ensure effective combustion by facilitating adequate air and fuel mixture formation.

In contrast, the modified camshaft profile exhibits a distinct change in valve timing behaviour. As depicted in the figure, the valve opening phase is entirely absent in the modified camshaft configuration. This modification was intentionally designed to prevent the intake valve from opening during critical phases of the intake stroke. By eliminating the valve opening at specific crankshaft angles, the modified camshaft aims to reduce the risk of backfire and premature combustion, particularly when operating in a hydrogen-gasoline dual-fuel mode.
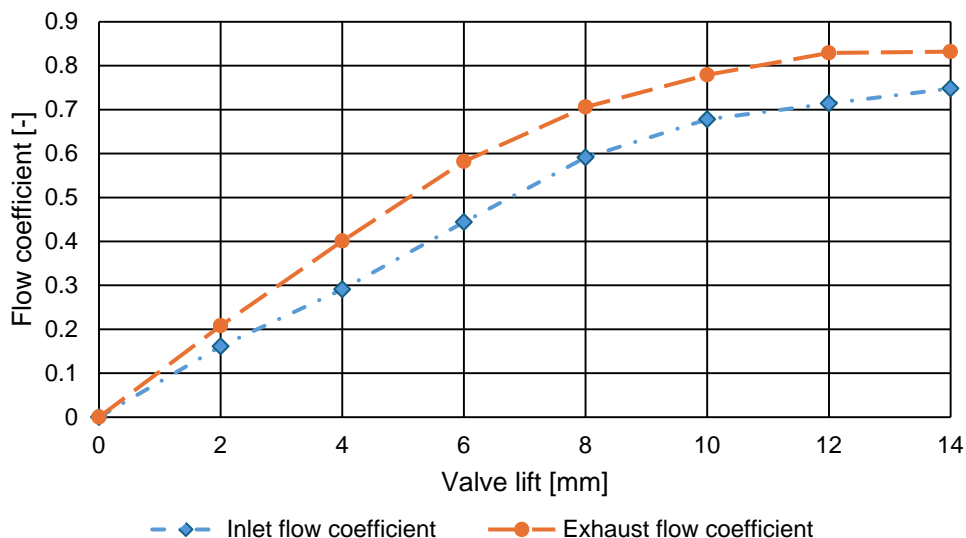
Figure 3. Valve lift coefficients

The flow coefficients of the ports were determined using a steady-state flow bench at a pressure difference of 6230 Pa (equivalent to 25 inches of H_2O). The calculations were based on the theoretical (isentropic) compressible mass flow for the given diameter, with the valve flow coefficients specifically calculated for the minimum valve seat diameter, dvdv

1.2.2   Simulation validation

In our previous research, we successfully validated the pure gasoline simulation within a standard AVL testbed environment. This validation process involved meticulous comparison between the measured values and those predicted by the simulation for key performance parameters, such as power, torque, and emissions. The results demonstrated a remarkable alignment, with deviations remaining under 3%, confirming the accuracy and reliability of the simulation model.

Building on this foundation, we advanced to the next phase of our research by developing a hydrogen-gasoline dual-fuel simulation. This phase aimed to explore the potential benefits and challenges associated with using hydrogen as a supplementary fuel in conventional gasoline engines. The dual-fuel simulation was meticulously configured to optimize the blend ratios, combustion timing, and fuel injection parameters, ensuring a balanced integration of both fuel types.

In the subsequent stage, we introduced a novel variable camshaft design specifically tailored for dual-fuel operation. This unique camshaft configuration was designed to optimize valve timing and lift profiles for eliminate the backfire problems and optimising the power and torque parameters at low RPM when operating on a hydrogen-gasoline mix. The modified simulation incorporated these advanced camshaft dynamics, allowing us to investigate the impact on engine performance and emissions under various load and speed conditions.

The experimental setup depicted in Figure 3 was instrumental in achieving these research objectives. This setup featured a highly controlled test environment equipped with precision sensors and data acquisition systems to monitor engine parameters in real-time.

This setup not only provided a robust framework for validating the dual-fuel simulation models but also facilitated the evaluation of the gasoline engine's performance and emissions characteristics under different configurations. The insights gained from these experiments will guide future developments in dual-fuel engine technology, with the potential to enhance fuel efficiency and reduce the environmental impact of internal combustion engines.
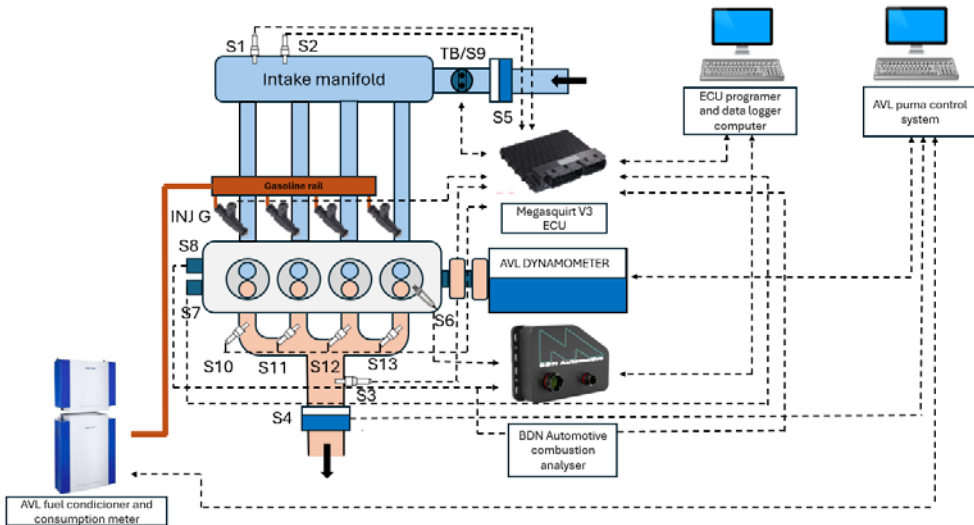
Figure 3. Testbed experimental setup

The unnamed elements of the block diagram are listed in Table 3.

Table 3 Modified camshaft parameters

S1	Intake air temperature sensor
S2	Intake manifold pressure sensor
S3	O_2 sensor
S4	AVL sesam i60 FTSII
S5	AVL flowsonix
S6	AVL indicator spark-plug and amplifier
S7	Camshaft position sensor
S8	Crankshaft position sensor
S9	Throttle position sensor
S10-S13	Exhaust teperature senores
TB	Throttle body

1.2.3 Fuel and air delivery system

Fuel was supplied to the engine using an advanced AVL fuel delivery system, which includes several key components for accurate measurement and control. The AVL fuel mass flow meter (735S) was utilized to measure the mass flow rate of the gasoline, ensuring precise fuel delivery throughout the testing process. The AVL flowsonix air flow meter was employed to monitor the intake air flow rat. To maintain consistent fuel properties, the AVL fuel temperature conditioner (752C) regulated the temperature of the gasoline to a stable 20[°C], minimizing variations that could affect combustion characteristics. The AVL fuel

module (7531.21) managed the fuel supply at a constant pressure of 3,5 [bar], ensuring a steady and reliable fuel flow to the engine under all operating conditions. Under the measurement the air temperature was 20[°C] and the air pressure was 1022 [hPa]

1.2.4   Exhaust Emissions Analysis

The engine's exhaust emissions were analysed using the AVL sesam i60 FTSII exhaust gas analysis system. This state-of-the-art equipment enabled the continuous measurement of critical exhaust gas components, including carbon monoxide (CO), carbon dioxide (CO_2), nitrogen oxides (NO_x), and unburned hydrocarbons (HC). By providing real-time emissions data, this system allowed for a detailed assessment of the engine's environmental impact under various operating conditions and fuel compositions.

1.2.5   Performance Measurements

Engine performance, including torque and power output, was measured using the AVL Dyno Road 200 dynamometer. This equipment is capable of precise torque and rotational speed measurements, providing accurate power output data across a wide range of engine speeds and loads. The dynamometer was crucial in evaluating the effects of different fuel blends and engine configurations on overall performance, helping to identify optimal operating parameters for the dual-fuel system.

1.2.6   Combustion Analysis System

To achieve maximum performance just below the knock limit and to facilitate the construction of an accurate simulation model, detailed combustion tests were conducted using a specialized combustion test system developed by BDN Automotive. This system was equipped with a CA-6 six-channel combustion analyser, which is capable of high-resolution data acquisition across multiple channels. An AVL indication spark plug and an AVL indicom charge amplifier were used to capture and amplify the combustion signals within the cylinder. The combustion analyser recorded data from all channels at a sampling rate of 1 MHz, allowing for the precise calculation of crank-angle-based combustion parameters, such as pressure, rate of heat release, and combustion duration.

The combustion test system utilized the signal from the original 60-2 pattern crank trigger wheel for accurate synchronization with the engine's operating cycle. This ensured that the combustion events were precisely correlated with the crank angle, enabling detailed analysis of the combustion process at various engine speeds and loads. The high sampling rate and multi-channel capability of the CA-6 analyser provided comprehensive insights into the in-cylinder phenomena, which were essential for refining the simulation model and improving the engine's performance and emissions characteristics.

1.2.7   Data Integration and Analysis

The data collected from the fuel delivery, exhaust emissions, and combustion analysis systems were integrated to provide a holistic view of the engine's behaviour. This comprehensive dataset was used to validate the simulation model, ensuring that the model accurately represented the real-world performance of the dual-fuel engine. By correlating the experimental data with the simulation results, we were able to identify key areas for optimization in both the engine hardware and the simulation model, leading to improved predictions and performance outcomes for the dual-fuel hydrogen-gasoline engine configuration.

Overall, the experimental setup and testing methodology provided a robust platform for investigating the complex interactions between hydrogen and gasoline in a dual-fuel engine. The insights gained from this research will contribute to the development of more efficient and environmentally friendly internal combustion engine technologies, supporting the transition towards sustainable mobility solutions.

2   SIMULATION RESULTS

The simulations confirmed that the custom camshaft design achieved a favourable balance between reducing backfire risk and maintaining engine performance, making it a promising solution for dual-fuel hydrogen-gasoline engines. Consistently illustrating the results of the simulation, we used a green line for petrol, a blue line for 20% hydrogen 80% petrol dual-fuel and an orange line for 20% hydrogen 80% petrol dual-fuel + modified camshaft values. Figure 4 represents the torque prediction.
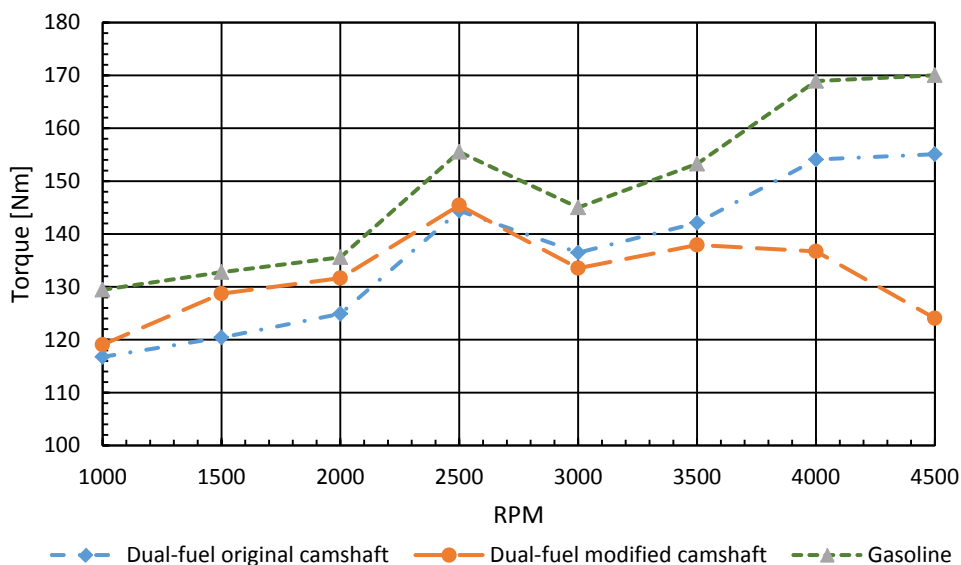
Figure 4. Torque prediction

It can be seen in the figure that using the new camshaft below 2500 rpm, we get higher torque values compared to the original camshaft in dual-fuel mode, but it still does not reach the torque level of gasoline mode. Between 2500 and 3500 rpm, we get slightly smaller torque values with the modified camshaft in dual-fuel mode, but above 3500 rpm, the torque curve drops drastically. Figure 5. represents the power prediction.
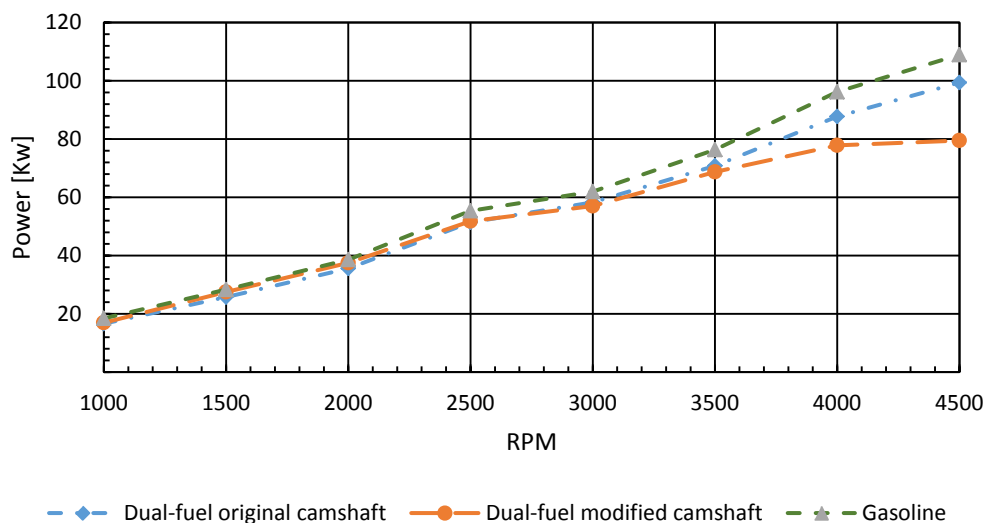
Figure 5. Power prediction

A significant difference between the performance curves can be observed above 3500 revolutions.
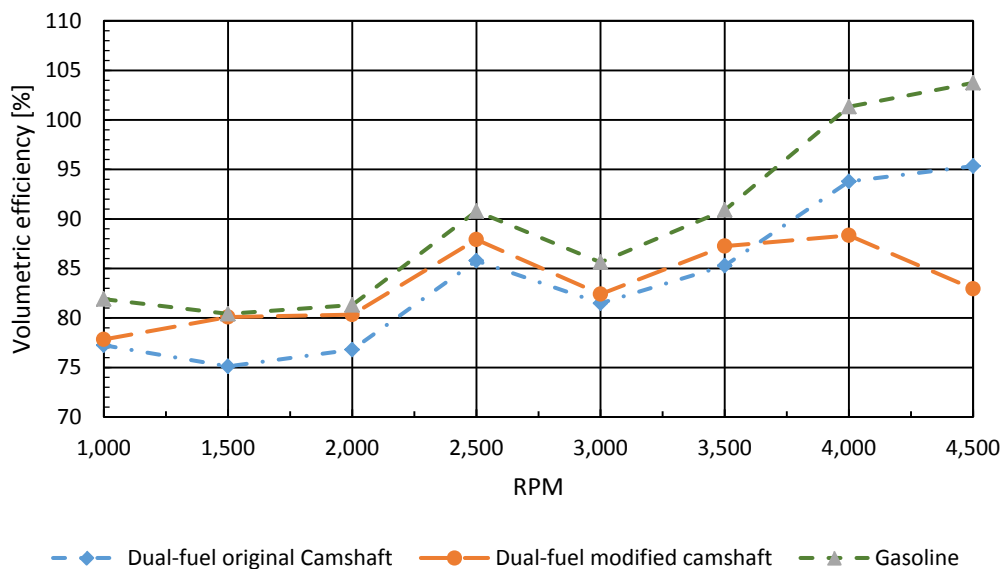
Figure 6. Volumetric efficiency prediction

The characteristics of the previously illustrated data and curves are explained by the change in the volumetric efficiency. At low revs, the volumetric efficiency with the modified camshaft is almost identical to that of pure gasoline. This is significant because hydrogen gas takes up a huge volume in the intake pipe in dual-fuel mode. On the other hand, the disadvantage of the modified camshaft is that the volumetric efficiency drops significantly at high revolutions, which has a great impact on the power and torque levels.
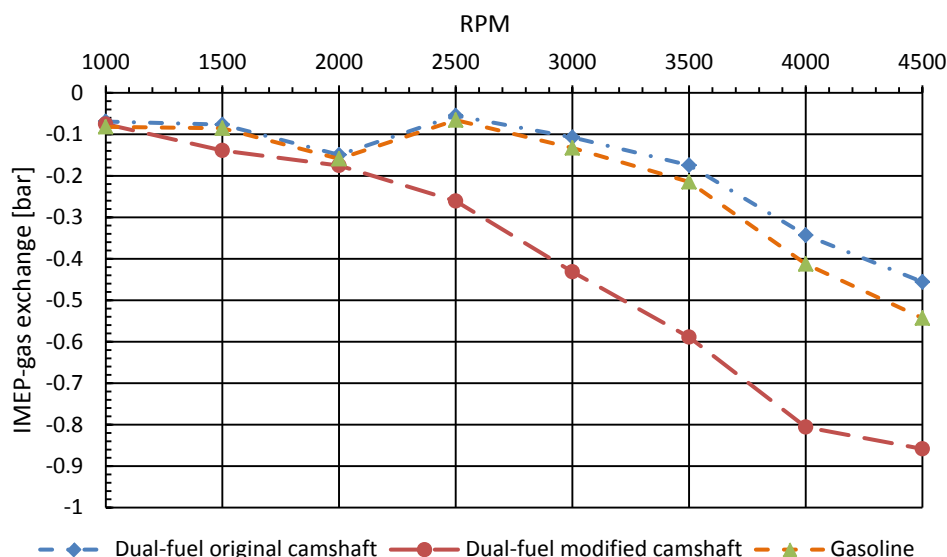
Figure 6. Indicated Mean Effective Pressure (IMEP)

In the modified camshaft configuration, the valve overlap is eliminated to prevent backfire and ensure more controlled combustion, especially when operating with hydrogen as a dual-fuel. However, this modification comes with a significant drawback: the absence of valve overlap at high engine speeds disrupts the natural flow of the intake and exhaust processes. Without valve overlap, the engine's ability to clear out residual exhaust gases is compromised, leading to increased reversion and decreased intake air charge. The modified camshaft design, with no valve overlap, significantly affects the engine's Indicated Mean Effective Pressure (IMEP) and overall performance, especially at high engine speeds.

3   CONCLUSIONS

This research investigated the effects of a custom camshaft design on the performance of a hydrogen-gasoline dual-fuel internal combustion engine using predictive simulations. The primary objective was to address the challenges associated with hydrogen integration, such as backfire, while optimizing overall engine performance. The proposed modification involved delaying the intake valve closure to reduce the likelihood of backfire and enhance combustion stability.

The simulation results demonstrated that the custom camshaft successfully minimized the risk of backfire and at lower engine speeds, improving combustion. However, the modification led to a noticeable decline in volumetric efficiency and IMEP gas exchange problems at higher revolutions, resulting in reduced power output and torque compared to the standard camshaft configuration. This trade-off highlights the inherent challenges in balancing performance and emissions in dual-fuel engines.

It is important to note that these findings are based on predictive simulations. In future work, we plan to validate these results by conducting experimental tests under real-world conditions using an AVL testbed. This will provide more comprehensive insights into the actual performance and emissions characteristics of the modified camshaft design in a practical setting, allowing for further refinement and optimization.

Despite the current limitations, the custom camshaft design showed promise in enhancing engine stability and emissions control under dual-fuel operation. The findings suggest that further optimization of camshaft timing and valve dynamics could field better performance outcomes without compromising the benefits of hydrogen addition. Future research should focus on refining camshaft profiles and exploring advanced control strategies to mitigate the limitations observed at higher engine speeds.

Overall, this study contributes valuable insights into the integration of hydrogen in ICE technology, supporting the development of more efficient and environmentally friendly automotive solutions. By addressing key challenges in dual-fuel engine design, the research paves the way for further innovations that could facilitate the widespread adoption of hydrogen as a sustainable energy source in the automotive sector.

REFERENCES

[1] Abdalla A.M., Hossain S., Nisfindy O.B., Azad A.T., Dawood M., Azad A.K.: "Hydrogen production, storage, transportation and key challenges with applications: A review", Renewable and Sustainable Energy Reviews, Vol. 173, (2023).

[2] Aghahasani M., Gharehghani A., Mahmoudzadeh Andwari A., Mikulski M., Pesyridis A., Megaritis T., Könnö J.: "Numerical Study on Hydrogen–Gasoline Dual-Fuel Spark Ignition Engine".Processes Vol.10, 2249 (2022).

[3] Dinçer A., Semiha Ö., Mustafa Kemalettin B.: "A review of hydrogen usage in internal combustion engines (gasoline-Lpg-diesel) from combustion performance aspect", International Journal of Hydrogen Energy, Vol. 45, 60, 35257-35268, (2020)

[4] D'Andrea T., Henshaw P., Ting D., "The addition of hydrogen to a gasoline-fuelled SI engine", International Journal of Hydrogen Energy, Vol. 29, 1541 – 1552, (2004)

[5] Farhad S., Meisam B., Seyed Vahid H., Anwar B.: "Multi-objective optimization of the engine performance and emissions for a hydrogen/gasoline dual-fuel engine equipped with the port water injection system, International Journal of Hydrogen Energy, Vol. 46, 10535-10547, (2021)

[6] Kenneth J. P., Ronald C. N., John B. H.: "Development and Evaluation of a Friction Model for Spark Ignition Engines", SAE Technical Paper Series, (1989)

[7] https://mymotorlist.com/engines/bmw/m43b18/

Intentionally blank

VEHICLE STABILITY ENHANCEMENT BASED ON WHEELS TORQUE DISTRIBUTION CONTROL FOR AN ACTIVE DIFFERENTIAL WITH ELECTROMECHANICAL ACTUATORS

Eid S. Mohamed[12]*

RESEARCH ARTICLE

ABSTRACT: High-performance vehicles use active differentials (AD) to maximize traction, stability, and safety by optimizing the torque distribution on the driving vehicle wheels. This work presents the torque distribution and speeds which are theoretically analyzed using mathematical models of the vehicle, driver, tire and drive train with an AD including the electromechanical actuation. The proposed controller is investigated using MATLAB/Simulink with AD as an external torque by an electromechanical actuation in a variety of driving scenarios, including straight lines under NEDC and J-turn input test with different road adhesions, to regulate lateral slide slip and vehicle yaw rate (YR) on different road adhesions can be obtained by an LQR controller. The results show that the AD can enhance the overall performance of the vehicle dynamics properties by transferring torque between the right and left wheels, which produces the direct yaw moment. The AD with integrated YR and vehicle side slip (VSS) control effectively improves vehicle dynamics and stability under different road maneuvers and adhesions.

KEY WORDS: *Active differential, motion stability, wheels torque distribution, yaw moment control, electromechanical actuators.*

[1] *Eid S. Mohamed, Faculty of Engineering, Mechanical Eng. Dept., Al-Baha University, KSA*
[2] *on Leave from Faculty of Engineering, Automotive dep., Helwan University, Egypt,*
e.mohamed@bu.edu.sa, eng_eid74@yahoo.com -(*Corresponding author)

POBOLJŠANJE STABILNOSTI VOZILA ZASNOVANO NA KONTROLI RASPODELE OBRTNOG MOMENTA TOČKOVA NA AKTIVNOM DIFERENCIJALU SA ELEKTROMEHANIČKIM AKTUATORIMA

REZIME: Vozila visokih performansi koriste aktivne diferencijale (AD) da maksimiziraju vuču, stabilnost i sigurnost optimizacijom raspodele obrtnog momenta na točkovima pogonskog vozila. Ovaj rad predstavlja raspodelu obrtnog momenta i brzine koje su teorijski analizirane korišćenjem matematičkih modela vozila, vozača, pneumatika i pogonskog sklopa sa AD uključujući i elektromehaničku aktivaciju. Predloženi kontroler je istražen korišćenjem MATLAB/Simulink-a sa AD kao eksternim obrtnim momentom elektromehaničkim aktiviranjem u različitim scenarijima vožnje, uključujući prave linije pod NEDC i J-turn ulaznim testom sa različitim adhezijama na putu, da bi se regulisalo bočno klizanje i skretanje vozila stopu (IR) na različitim adhezijama na putu može da dobije LKR kontroler. Rezultati pokazuju da AD može poboljšati ukupne performanse dinamičkih svojstava vozila prenosom obrtnog momenta između desnog i levog točka, što proizvodi direktan moment skretanja. AD sa integrisanom IR i kontrolom bočnog klizanja vozila (VSS) efikasno poboljšava dinamiku i stabilnost vozila pri različitim manevrima i prianjanjima na putu.

KLJUČNE REČI: *Aktivni diferencijal, stabilnost kretanja, raspodela obrtnog momenta točkova, kontrola momenta skretanja, elektromehanički aktuator*

VEHICLE STABILITY ENHANCEMENT BASED ON WHEELS TORQUE DISTRIBUTION CONTROL FOR AN ACTIVE DIFFERENTIAL WITH ELECTROMECHANICAL ACTUATORS

Eid S. Mohamed

INTRODUCTION

- ### *Background of vehicle stability*

Most vehicle dynamic control systems available on the market are brake-based and apply individual wheel braking forces using anti-lock braking system hardware to preserve vehicle stability in emergencies. These dynamic stability control (DSC) systems employ differential tire brake forces between the vehicle's wheels to generate the required yaw moment for correction. These systems are highly effective when the handling limit is approached, but they are undesirable for everyday driving conditions due to the control action's direct impact on the longitudinal dynamics of the vehicle, which affects the vehicle's longitudinal performance and distracts the driver [1, 2]. Early research on active safety and vehicle stability systems mostly concentrated on enhancing the motion's longitudinal dynamics, namely on more efficient traction control (TC) and anti-braking (ABS) systems active front steering (AFS) systems and yaw motion control (YMC). By optimizing the tractive and the tire and the road's lateral forces, (LSD) systems not only keep the wheel from slipping but also increase vehicle stability and steerability [3,4]. To maintain vehicle stability in harsh handling conditions, an AD design approach and rescheduled active steering control were created. The effectiveness of the chosen modeling and controller design methods in enhancing the ability of the vehicle to handle when cornering on roadways by reducing the lateral forces between the tire and the pavement with different adhesion coefficients and during variable-speed operations was demonstrated through simulations [5, 6].

- ### *Overview of an active differential*

Other actuation technologies that can offer more stability without the obtrusiveness of a brake-based system are being explored. One such option is active limited slip differentials (ALSDs), which provide electronically regulated torque transfer between the driven wheels. By generating a yaw moment through controlled torque transfer across an axle, vehicle stability can be increased. This increase in stability can be accomplished less invasively than with a brake-based control system because wheel torque is reapportioned rather than decreased. An automotive differential mechanism's primary function is to prevent the traction wheel from slipping when the car turns a bend. This function is often carried out using a planetary gear, which maintains an equal torque distribution while permitting varying rotational speeds to the wheels to which the differential is linked.

Compared to a regular differential, a limited slip differential might (LSD) have numerous advantages. By biasing torque to the wheel with superior traction, LSD helps improve the overall traction and handling performance of the vehicle. This can be especially beneficial in situations such as driving on slippery or uneven surfaces, where one wheel may lose traction more easily than the other. Better handling and mobility qualities may result from this. Because of their design, traditional LSD has inherent restrictions. Any vehicle's mobility and handling can be maximized by electrically regulating the differential's output **[7-9].** Companies in the automotive industry and literature have long recognized the impact of LSD on the dynamics of the vehicle. The industry has long adopted passive self-locking

mechanisms. The automotive industry and businesses have undertaken numerous initiatives in recent years to use regulated, semi-active, or ADs to get around these restrictions **[10, 11].**

Limited slip differentials (LSDs), which can provide an internal locking torque that enables the differentiation of the torque output and the generation of a yaw moment on the vehicle, are key characteristics of torque distribution systems. By dynamically adjusting the torque distribution, controllable LSD can enhance vehicle stability and cornering performance. For example, during cornering, if the inside wheel loses traction and starts to spin, the LSD can transfer more torque to the outside wheel, which has better grip. This helps to prevent excessive wheel spin and maintain traction, allowing the vehicle to effectively and safely navigate the turn. Furthermore, controllable LSD can also help to mitigate under steer and over steer tendencies. Under steer occurs when the front wheels lose grip and the vehicle tends to push wide in a turn. By transferring more torque to the rear wheels, controllable LSD can increase rear traction and improve cornering performance. [12, 13]. Adaptive systems known as magnetorheological (MR) devices can change their characteristics by applying a regulated magnetic field with an electrical power signal. To achieve this goal, countless attempts have been made to create LSDs and their control systems to satisfy the Figure 1 shows the classification of clutch types, they can be roughly categorized as electromagnetic clutches, pneumatic clutches and brakes, hydraulic clutches, and mechanical clutches. These uses clutches mechanically, hydraulically, pneumatically, and electromagnetically, as their names imply.
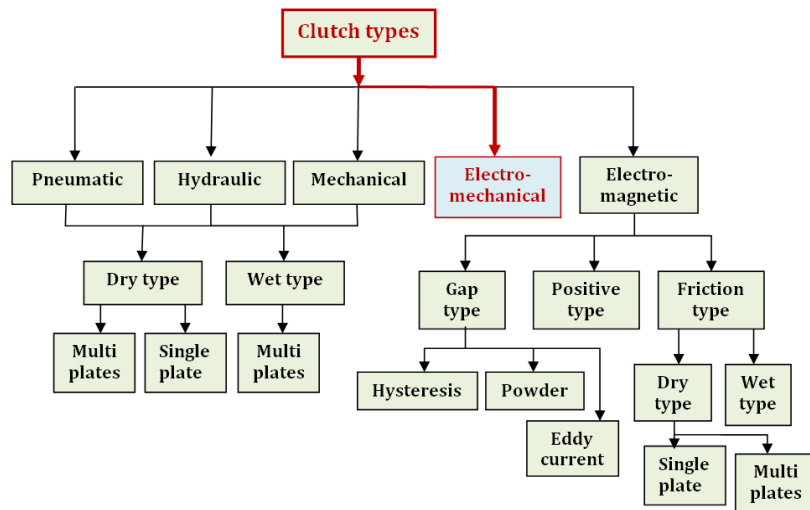
Figure 1: Classification of clutch types

Figure 2 shows the diagram of a conventional differential (CD) and active differential (AD), a CD is a fixed distribution of the drive torque with a conventional rear differential; a conventional rear differential consists of an angled drive and a differential gear and always distributes the drive torque equally (50:50) to both sides. Different rotational speeds are balanced out. The other gear ratios for the various vehicle models are achieved by the different number of teeth on the drive pinion and crown gear. The speed of the drive wheels can differ from each other because of the various distances they cover when cornering. The drive torque is always distributed equally to both drive wheels and does not therefore generate any yawing.

Vehicle stability enhancement based on wheels torque distribution control for an active differential with electromechanical actuators

19

These benefits are counterbalanced by a major disadvantage if the tire-road adhesion is different at the two wheels. The propelling forces that are to be transferred to the road are then limited to the lower of the two potential adhesion levels at the drive wheels. If the adhesion ratio is unfavorable on one side, it means that a vehicle (without electronic dynamic driving system) would not be able to move off. The drive torque would be converted into useless rotational acceleration for the wheel with the lower potential adhesion level, while the higher potential adhesion of the second drive wheel remains unexploited. The AD with distribution of the drive torque by the rear differential with mechanical locks (limited-slip differential).

a.   Conventional differential

b. Active limited slip differentials
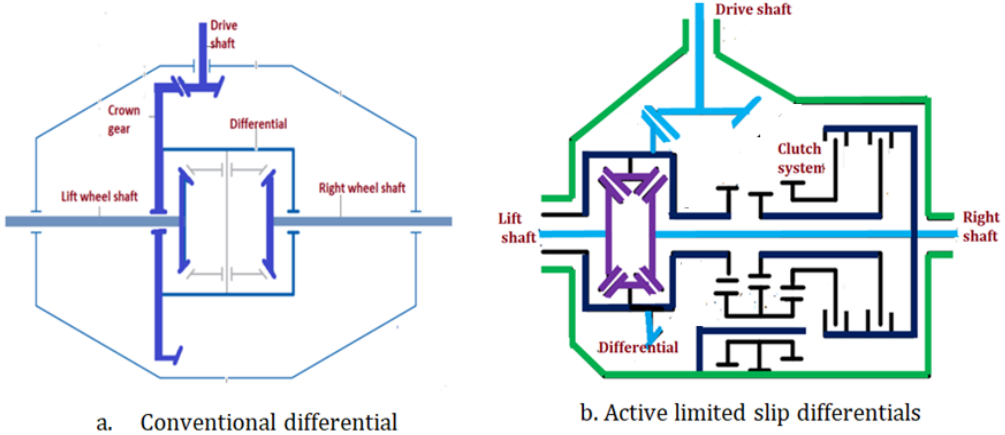
Figure 2: Schematic diagram of a CD and AD

1.   VEHICLE DRIVE TRAIN MODEL

The torque generated by the ICE engine and sent to the vehicle's drivetrain via AD is represented by T_e in Figure 4.The friction torques (T_{cr} and T_{cl}) are represented as simple Coulomb friction proportional to the clutch compression force (F_{cr} and F_{cl}). By imposing the dynamic equilibrium of the planetary and solar gears, differential housing, gearbox, and rotary engine components, the equilibrium differential equations characterizing the AD dynamics were found using both Lagrange and Newton techniques. The dynamic equations are reduced to only three by applying the standard kinematic relations between the angular velocities of the solar, planetary, and differential housing gears. These formulas allow the motor torques (T_{rs}, T_{ls}) and angular velocities (ω_r, ω_l) on the left and right solar gear. The vehicle dynamic equilibrium equations:

$$J_e \ddot{\theta}_e = T_m - T_t \tag{1}$$

$$J_t \ddot{\theta}_t = T_t - T_p \tag{2}$$

$$J_g \ddot{\theta}_g = I_g T_p - T_d \tag{3}$$

$$J_d \ddot{\theta}_d = I_d T_d - (T_{wl} + T_{wr}) \tag{4}$$

$$J_{eq}\ddot{\theta}_{ax} = (T_{wl} + T_{wr}) - (F_{wl} + F_{wr})R_w - (F_{cl} + F_{Cr})R_p \tag{5}$$

where $\ddot{\theta}_e$, $\ddot{\theta}_t$, $\ddot{\theta}_g$, $\ddot{\theta}_d$, and $\ddot{\theta}_{ax}$ are the angular accelerations of the engine output shaft, torque converter axles, planetary gear box, differential gear and axle of drive wheels. J_e, J_t, J_g, J_p, J_d, and J_{eq}, are moment of inertia of the engine, torque converter axles, planetary gear, differential gear and axle of drive wheels components. T_e, T_t, T_p, T_d, T_{wl}, and T_{wr} are the engine torque, torque converter torque, planetary gear torque, differential gear torque, left and right wheels torque. F_{wl}, and F_{wr} are the left and right wheels force. F_{cl}, F_{cr} are the left clutch force and right clutch force of the AD. I_g, I_d are the transmission ratio in gearbox and the final drive ratio.
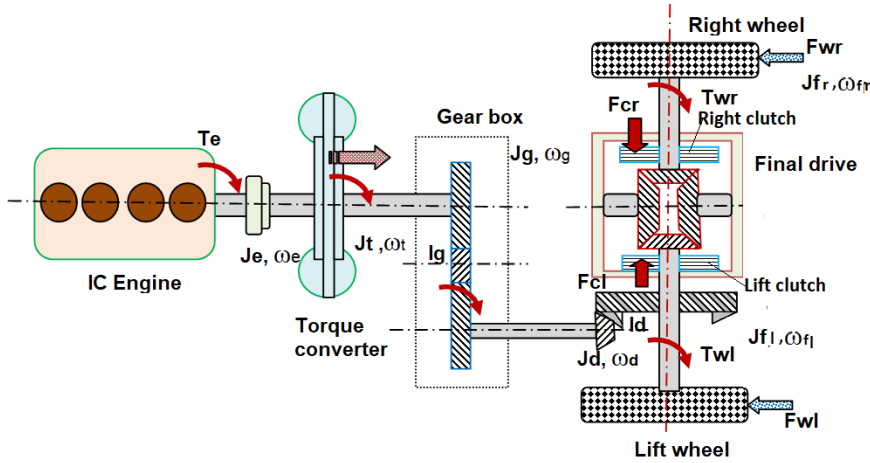
Figure 3: The vehicle driveline model

1.1   Engine model

The engine is represented model as the torque actuator, the model constant inertia that is coupled to the flywheel and clutch via the crankshaft. The engine's net torque, taking friction and torque losses into account, is represented as torque T_e. The engine model is derived from existing experimental data and is quasi-static. A look-up table is used to derive engine torque as a function of engine throttle position, as seen in **Table 1**.

Table 1: IC Engine torque map

Engine torque (N.m)		Throttle position (θ %)							
		5	**10**	**15**	**20**	**25**	**30**	**40**	**50**
Engine speed (N_e rpm)	**100**	65	80	90	117	109	110	118	125
	1500	70	96	100	132	133	134	136	140
	2000	60	110	120	133	141	142	144	150
	2500	45	87	102	133	147	148	150	155
	3000	36	74	99	133	153	159	168	165
	3500	22	60	88	136	152	161	175	178
	4000	12	55	83	126	150	160	177	182

Vehicle stability enhancement based on wheels torque distribution control for an active differential with electromechanical actuators

21

4500	9	51	77	140	155	179	186	199
5000	5	43	75	136	175	194	205	220
5500	0	33	71	101	147	167	185	200
6000	0	22	68	94	136	161	160	193
6500	0	18	66	88	130	140	155	178

1.2 *Torque converter model*

A centripetal impeller and turbine with a lock-up clutch serves as the torque converter in power train. The following criteria are used to assess the torque converter transmission characteristics:

$$\omega_t = i_s \omega_b \qquad (6)$$

$$T_b = \lambda_b \rho g \omega_b^2 D^5 \qquad (7)$$

Where ω_t and ω_b are turbine and impeller speeds and, T_b is impeller torque, λ_b is torque capacity coefficient of torque converter, ρ is oil density, η_t is the transmission efficiency.

The power loss (P_t) is expressed by:

$$P_t = T_b \omega_b (1 - \eta_t) \qquad (8)$$

1.3 *Active differential model*

An electronically controlled system regulates the torque distribution between the left and right wheels of the driving axle, limited slip differential. Limited slip functionality is provided via a multi-plate dry clutch positioned between the differential enclosure and the output shaft. Clutch engagement starts the torque transfer from the housing to the output shaft. This makes it possible to individually modify the torque magnitude of each output shaft. The clutch torque needs to be changed to produce the appropriate vehicle yaw dynamics under particular driving circumstances.

A Simple diagram of an AD is shown in **Figure 4** for easy comprehension. Electromechanical actuators activate the friction plates. T_g represents the input driving torque that is transferred to the differential by the gearbox, whilst T_{wr} and T_{wl} represent the torques at the output to the left and right shafts, respectively.

$$T_{wr} = \frac{T_g - T_{cr} + T_{Cl}}{2} \qquad and \ T_{wl} = \frac{T_g - T_{cl} + T_{Cr}}{2} \qquad (9)$$

The variation in torque between the clutches on the left and right is known as the controller output torque ($T_{diff.}$)

$$T_{deff} = T_{Cr} - T_{Cl} \qquad (10)$$

Where $T_{cr} = F_{cr} R_p$ and $T_{cl} = F_{cl} R_p$

The subsystem was dedicated to specific driving conditions, like starting on the AD. In this situation, the adhesion of one driven wheel is low (low ϕ) surface, such as ice or mud, and it is unable to transmit the driving torque to the earth.. All of the driving power would be dispersed by a free differential while the automobile is stationary by allowing the wheel on low ϕ to spin (**Figure 5**).
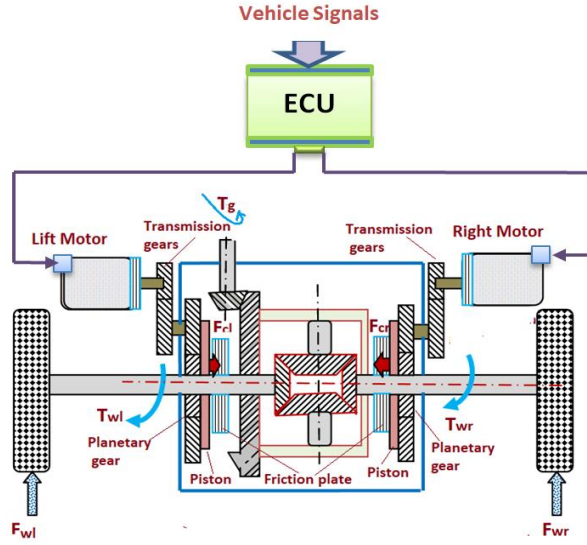
Figure 4: *A Simple diagram of an active diffe*rential

a.   Free differential
b.   Active differential
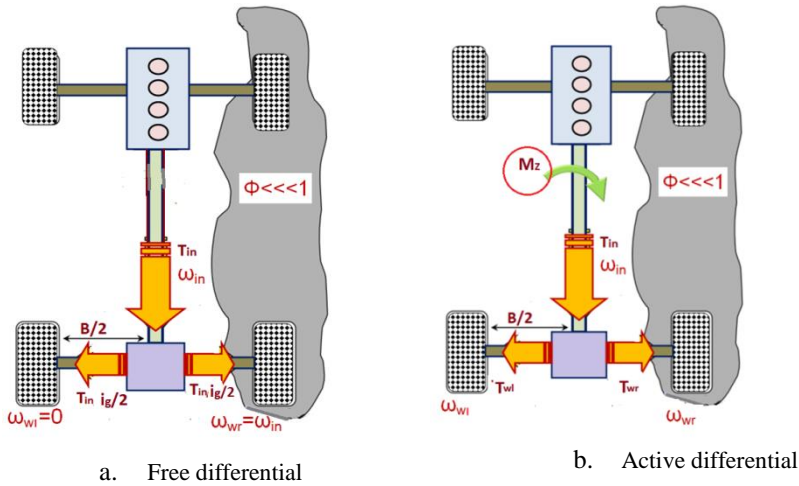
Figure 5: *Working principle of free and active differential*

1.4   *Electromechanical actuator model*

A DC motor's electrical circuit is made up of a voltage source (the controller provides the voltage input), a resistor, an inductor, and a back EMF that is proportionate to the motor's RPM connected in series. An electromechanical actuator (EMA) regulates the speed ratio, and the DC motor's power consumption is stated in:

$$P_m = \frac{V_o I_o}{\eta_m} \tag{11}$$

2.

Vehicle stability enhancement based on wheels torque distribution control for an active differential with electromechanical actuators

23

where P_m denotes power consumed by the DC motor, V_o operating voltage of the motor, I_o operating current, and η_m charge–discharge efficiency of the battery. A DC motor with a permanent magnet is selected as the actuator motor of the EMA's. Additionally, the formulae for torque and voltage balancing are explained in Eqs. (5) and (6), respectively, as follows

$$V = IR + L\frac{dI}{dt} + K_e\omega_m \tag{12}$$

3. $$J_m\frac{d\omega_m}{dt} = K_T I - T_L \tag{13}$$

where R is the DC motor armature resistance, L is motor armature inductance, K_e is back-EMF coefficient, J_m is the output shaft moment of inertia, ω_m is the output shaft angular velocity, K_T is the torque coefficient, and T_L is the DC motor torque load.

2 VEHICLE DYNAMIC MODEL

A 4-wheel vehicle handling model that accounts for tire non-linearity and vehicle roll dynamics must be developed because handling studies of standard AD systems usually use a road vehicle bicycle model, which ignores lateral load shift and tire saturation limit. Make use of the coordinate system for vehicles depicted in **Figure 6 (a).**

Front, Right wheel $$F_{fr} = W_f - \frac{ma_x h_{cg}}{2L} + \frac{ma_y h_{cg} b}{2T_f L}$$

Front, Left wheel $$F_{fl} = W_f - \frac{ma_x h_{cg}}{2L} - \frac{ma_y h_{cg} b}{2T_f L}$$

$$\tag{14}$$

Rear, Right wheel $$F_{rr} = W_r + \frac{ma_x h_{cg}}{2L} + \frac{ma_y h_{cg} a}{2T_r L}$$

Rear, Left wheel $$F_{rl} = W_r + \frac{ma_x h_{cg}}{2L} - \frac{ma_y h_{cg} a}{2T_r L}$$

The traction force distribution is described as a four-wheel model with three degrees of freedom: longitudinal, lateral, and yaw. The following expression can be used to illustrate the equations that govern both lateral and longitudinal motion:

$$m\dot{V}_x = ma_x = \sum F_x = F_{xr} + F_{xl} \tag{15}$$

$$ma_y = F_{yfr}\cos(\delta_f) + F_{yfl}\cos(\delta_f) + F_{yrr} + F_{yrl} \tag{16}$$

$$mV(\dot{\beta} + \Omega) = \sum F_y = F_{yfr} + F_{yfl} + F_{yrr} + F_{yrl} \tag{17}$$

where m is the vehicle mass; a_x and a_y are the longitudinal and lateral accelerations of vehicle, respectively and δ_f is the front steering angle. The slip angle, Ω is the YR, F_{yfl}, F_{yfr} is the cornering force of the front tires, F_{yrl}, F_{yrl} is the cornering force of the rear tires, and V_x is the vehicle velocity.

2.1 *Reference model*

Based on earlier studies, a simplified two-DOF vehicle model is typically developed to explain the lateral dynamics of the vehicle, using the yaw rate Ω and the VSS angle β as the

system's states. **Figure 6 (b)** displays the yaw plane reference model system. One way to characterize the 2DOF model is

$$\dot{\beta} = \left[-\frac{2(C_f + C_r)}{mV_x} \right] \beta + \left[-\frac{2(aC_f - bC_r)}{mV_x^2} - 1 \right] \Omega + \frac{2C_f}{m} \delta_f \tag{18}$$

$$\dot{\Omega} = \left[-\frac{2(aC_f - bC_r)}{I_z V_x} \right] \beta - \left[\frac{2(a^2 C_f + b^2 C_r)}{I_z V_x} \right] \Omega + \frac{2aC_f}{I_z} \delta_f + \frac{M_z}{I_z} \tag{19}$$

Equations for linear single-track models are:

$$\begin{bmatrix} \dot{\beta} \\ \dot{\Omega} \end{bmatrix} = \begin{bmatrix} \dfrac{2(C_f + C_r)}{mV_x} & \left[-\dfrac{2(aC_f - bC_r)}{mV_x^2} - 1 \right] \\ \left[-\dfrac{2(aC_f - bC_r)}{I_z V_x^2} - 1 \right] & \left[\dfrac{2(a^2 C_f + b^2 C_r)}{I_z V_x} \right] \end{bmatrix} \begin{bmatrix} \beta \\ \Omega \end{bmatrix} + \begin{bmatrix} 0 \\ \dfrac{1}{I_z} \end{bmatrix} M_z + \begin{bmatrix} \dfrac{2aC_f}{m} \\ \dfrac{2aC_f}{I_z} \end{bmatrix} \delta_F \tag{20}$$

The vehicle motion in longitudinal direction can be written as:

$$m\dot{V}_x = ma_x = \sum F_x = F_{xr} + F_{xl} \tag{21}$$

The computer simulation of YR tracking control is conducted in Matlab/Simulink, the vehicle parameters, drive line parameters and DC motor parameters used are taken on **Table 1.**

a. The vehicle coordinates and force analysis

b-DOF yaw plane reference model
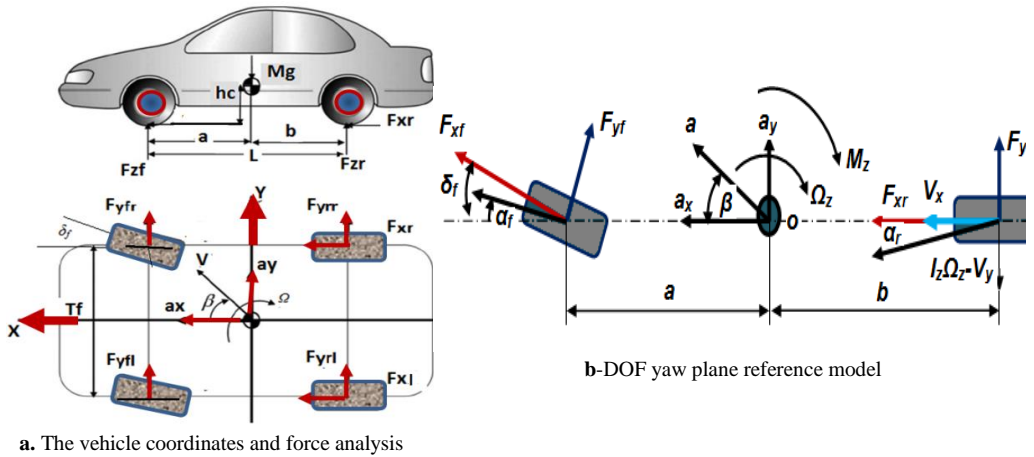
Figure 6: Vehicle dynamic and reference models

2.2   Vehicle path following Model

The single-track model and the state variables in terms of position and orientation error are used to create a dynamic path-following model. **Figure 7(a)** shows the configurations of the desired and actual vehicle orientations. The vehicle orientation on its intended path is represented by the x_d, y_d frame, whereas the x-y frame shows the vehicle orientation on its actual path **[21]**. At the preview point, the anticipated lateral position is:

$$Y(t + t_p) = Y(t) + a_y \frac{t_p^2}{2} + V_x \Omega t_p \tag{22}$$

where, t_p denotes the driver preview time, $y(t+t_p)$ the predicted vehicle lateral position at the preview point, Ω vehicle yaw angle. The desired position vector R_d can be defined in the mobile frame *x–y* as:

$$\vec{R_d} = x_d \, \vec{i} + y_d \, \vec{j} \qquad (23)$$

The goal is to minimize both the lateral position and orientation errors relative to the desired path, in order to provide a desired path control. The orientation error and its derivative can be written as:

$$\Delta\Omega = \Omega_{des} - \Omega_{act}$$
$$\dot{\Delta\Omega} = \dot{\Omega}_{des} - \dot{\Omega}_{act} \qquad (24)$$

where $\dot{\Omega}_{des}$ is the rate of change of the desired orientation of the vehicle and is defined as:

$$\dot{\Omega}_{des} = \frac{V_x}{R_{des}} \qquad (25)$$

where R_{des} is the radius of curvature of the desired path.

2.3   Vehicle tyre model

As seen in **Figure 7 (b)**, a simplified quarter car vehicle model experiencing a driving move or completely straight line regenerative braking has been taken into consideration. The torque equation for adaptive DYC are imposed by mean of appropriate motor actuators, the DYC is actuated through the rear axle tyres characteristic.

$$J_{wrl} \, \dot{\omega}_{rl} = T_{rl} - F_{xrl}.R_w$$
$$J_{wrr} \, \dot{\omega}_{rr} = T_{rr} - F_{xrr}.R_w \qquad (26)$$

Where V_x represents the longitudinal velocity, $\omega_{rl,}$ ω_{rr} is the angular rotational speed of Left/right wheel, T_m represents the traction torque generated by the motor, R_w, J_w wheel radius, inertia momentum , $F_{x,rl}$, $F_{x,rr}$ Rear left/right tyre longitudinal forces, T_{rl}, T_{rr} Left/right wheel tractions

a. predictive driver model
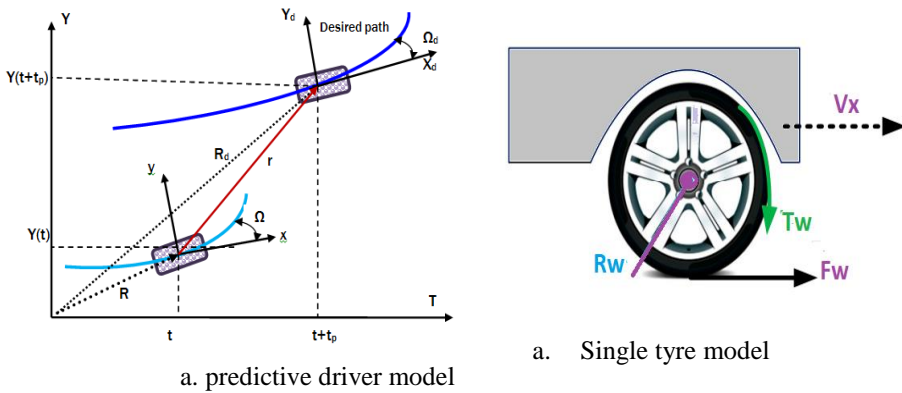
a.   Single tyre model

Figure 7: *vehicle path and tyre models*

Using tyre magic formula, the actual longitudinal tyre force (F_{xi}) can be obtained. The tyre magic formula expresses the tyre longitudinal force (F_{xi}), the lateral force (F_{yi}), and the aligning torque (M_{zi}) as a function of the tyre side slip angle (α_i) and the longitudinal slip ratio (λ_i). The general form of the tyre magic formula is as follows **[16]:**

$$y(x) = D\sin\left[C\tan^{-1}(Bx - E(Bx - \tan^{-1}(Bx)))\right]$$
$$Y(X) = y(x) + S_v$$
$$x = X + S_h$$

(27)

the slip ratio (λ) can be rewritten as

$$\lambda = \frac{V_x - V_w}{V_x} = \frac{V_x - \omega.R_w}{V_x}$$

(28)

where the output variable $y(x)$ represents the tyre longitudinal force, lateral force, and aligning moment, and the input variable (x) may represent α_i or λ_i. The coefficient B is the stiffness factor, C the shape factor, D the peak factor, and E the curvature factor. S_h and S_v are the horizontal and vertical shifts, respectively. For a given tyre, using experimental data, these coefficients are tuned. These coefficients can be tuned easily by the genetic algorithm method. $Y(X)$ is a changed coordinate system to enable an offset with regard to the origin in the curve produced by the magic formula.

2.4   *Design of control system*

The goal of the control system to ensure the car travels along the intended route with side-slip angle and YR values that are almost at their intended levels by AD traction torque distributions. Furthermore, even when the driver directives are present, the controller must function as intended. An ideal controller with the construction depicted in **Figure 8** is created for this objective. It is divided into three sections: (YMC), driver dynamics, and vehicle dynamics.

2Optimal design

The Linear Quadratic Regulator (LQR) approach serves as the foundation for the control system that this research suggests. In this section, the best controller for a linear tracking problem is designed using the 6DOF linear vehicle model. For the purpose of controlling vehicle dynamics, the performance index usually takes the following basic form:

$$J = \frac{1}{2}\int_0^\infty \left[w_1(\Omega - \Omega_d)^2 + w_2 M_Z^2 + w_3 T_{diff}^2 + w_4 v^2 + w_5(\delta_f - \delta_d)^2\right]dt$$

(29)

where T_{diff} is the AD torque, M_z is the vehicle yaw moment, Ω_d is the desired YR, δ_d is the desired steering angle and w_1, w_2, w_3, w_4, and w_5 are the weighting parameters used to balance each term's relative relevance in the equation. The optimal control rule is composed of the disturbance feed-forward signal related to the road specification and the state variable feedback signal, which is represented as:

$$M_Z = K_\Omega \Omega + K_\delta \delta + K_\beta \beta + K_v v$$

(30)

where $K_\Omega, K_\delta, K_\beta$ and K_v are known as the state gains.

2.4.2 Path tracking control

The closed-loop system of driver/vehicle interaction for the path-tracking problem is finished using the driver model that is shown below. One widely used approach is to define human control behavior as a transfer function and treat it as a linear continuous feedback control. It is possible to justify PID controllers for this reason.

The transfer function of the driver model is given by [16]

$$Y(t+t_p) = Y(t) + a_y \frac{t_p^2}{2} + V_x \Omega t_p$$

(31)

The actual YR control techniques based on the existing control loop to accomplish the parking trajectory tracking function. The short steering angle control algorithm is presented in this section. The difference between the wheels slip command and vehicle body slip feedback is used by the controller to determine the AD motor current command. The linear 2DOF model of the dynamic system can be defined using the state space form that follows:

$$\begin{cases} \dot{x} = Ax + Bu \\ y = Cx \end{cases}$$

(32)

where

$$x = \begin{bmatrix} \beta & \Omega \end{bmatrix}^T, \ u = \begin{bmatrix} \delta_f & M_z \end{bmatrix}^T \text{ and } y = \begin{bmatrix} \Omega & a_y \end{bmatrix}^T$$

where M_z indicates input of yaw moment control (YMC), It is produced by the AD motors' autonomous torque management., and δ_f is the steering angle.

The tracking error is represented by the variable e, which is given to the PID controller, which calculates the error between the actual output $Y(t)$ and the desired input value $Y(t+t_p)$. The proportional gain (KP), integral gain (*KI*) and derivative gain (*KD*), the control gains are evaluated from error signal e will the signal u just past the controller [7, 19]

$$u = K_P e + K_I \int e \, dt + K_d \frac{de}{dt}$$

(33)

The values of KP=2500, KI=7.8, and KD=230 were chosen in order to achieve the necessary damping ratio, and each of these parameters was adjusted until the appropriate overall response was achieved.
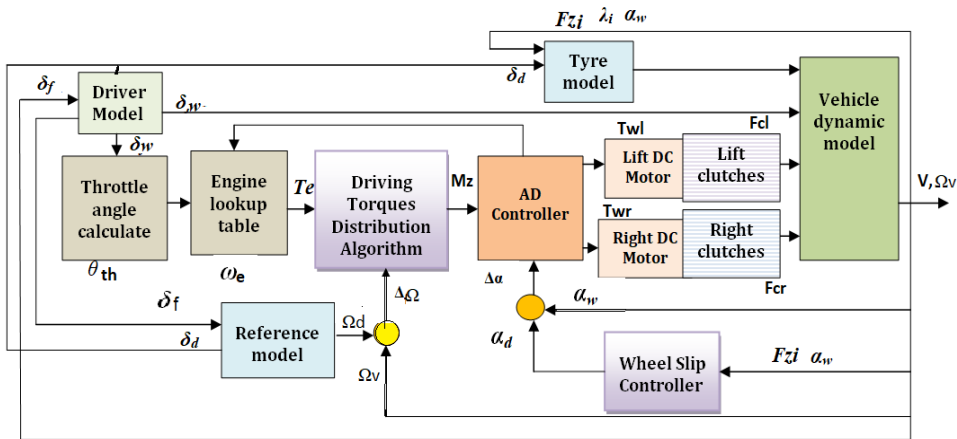
Figure 8: *Block schematic of the vehicle stability control system overall*

Table 2: Simulation model parameters

No.	Parameter	Notation	Unit	value
The parameters of vehicle model				
1	Sprung mass (mass vehicle)	m	kg	1300
2	moment of inertia about z axis	I_z	Kg.m^2	600
3	Wheel base	L	m	2.3
4	Distance of CG from front axle	a	m	1.15
5	Distance of CG from rear axle	b	m	1.26
6	Height of CG from ground	h_{cg}	m	0.4
7	Wheel radius	R_w	m	0.278
8	Track width axles	T	m	1.24
9	Cornering stiffness front and rear wheels	C_f C_r	N/rad	54000 35200
10	Max. motor torque at speed	T_{max}/N_e	Nm/rpm	210/5200
11	Tyre–wheel roll inertia	J_w	kg m^2	1.2
The driveline model				
1	Engine moment of inertia	J_e	kg m^2	4.98
2	Torque converter axles inertia	J_t	kg m^2	0.46
3	Planetary gear moment of inertia	J_p	kg m^2	0.26
4	Differential gear inertia	J_d	kg m^2	0.18
5	Gear transmission ratio	I_g	-	1
6	Final drive ratio	I_d	-	4
DC motor model				
1	moment of inertia	J_m	kg m^2	0,022
2	Maximum Current	I	A	200
3	Inductance	L	μH	18
4	Resistance	R	Ω	0.06
5	Torque coefficient	K_T	Nm/A	1.25
6	Back-EMF coefficient	K_e	V/rad/sec	0.5

3   SIMULATION RESULTS

There are two cases to discuss the results. First, the car is exposed to a road with a different friction between the right and left wheels, and the car drives in a straight line. Secondly, the car is exposed to a curved road. The typical curves of the lateral tire force in relation to tire VSS are displayed in **Figure 9** for different frictional road surface conditions, including dry asphalt (μ=0.8), dry cobblestone (μ=0.7), wet asphalt (μ=0.4), and snow (μ=0.2). In areas with a small tire slip angle (up to 4 degrees, for example), the lateral tire forces rise linearly as the slip angle increases. By adjusting the front steering angle, yaw stability can be improved.
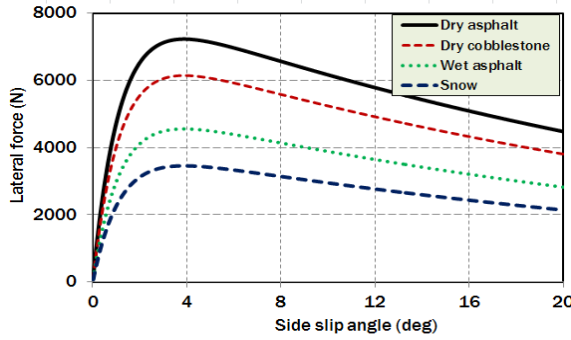
Figure 9: The tire lateral force characteristics with various road surfaces

3.1   Vehicle motion in straight line

The car underwent new European Driving Cycle testing (NEDC). Following the urban cycle, this one involves driving at a half-steady pace with occasional idling, accelerations, and decelerations. NEDC is made up of the urban driving cycle (UDC) and the extra-urban driving cycle (EUDC), which cover driving conditions on city streets and highways, respectively. UDC simulates an average speed of 18.9 km/h and a maximum speed of 60 km/h. A low-speed urban cycle lasting 780 seconds is repeated four times over the entire cycle, as shown in Figure. 10. With a mean speed of 63 km/h, the EUDC can reproduce a maximum speed of 120 km/h.

The vehicle power train is operated by a New European Driving Cycle (NEDC), which also determines the desired vehicle speed (V_d). A PID driver model is used to assess the throttle valve opening (θ_{th}) and pedal position (θ) by comparing the desired and actual vehicle speed (V) in order to choose engine (Ne-Te) operation values. In order to choose the best torque of wheels, an engine lockup table is utilized along with the real vehicle speed and engine characteristics (Ne-Te). The torque is expressed between left and right wheels according to AD motors torque.

The simulations presented in this section refer to a vehicle in straight line throughout the new European drive cycle (NEDC) with vehicle speed according to NEDC. Figure 10 shows the full cycle of NEDC input with four repetitions of a 780-second, low-speed urban cycle are made. With a mean speed of 63 km/h, the EUDC can reproduce a maximum speed of 120 km/h.

Figure 11 illustrates of the vehicle wheels torques and speed with dry asphalt (Φ=0.8) under NEDC. When all wheels of the vehicle are exposed to the same surface adhesion on dry asphalt, torque is distributed equally to the left and right wheels ($T_{wl}=T_{wr}$) see Figure 11 (a), and under the same conditions, the rotational speed of the right and left wheels is equal ($\omega_{wl}=\omega_{wr}$) see Figure 11 (b).

Figure 12 presents the vehicle wheels torque and speed with the CD with a slippery road. When the vehicle right wheels are exposed to a slippery road wet asphalt (μ=0.4) and the left one is exposed to a dry road dry asphalt (Φ=0.8), the rotational speed of the right wheels increases but the left wheels speed decreases, causing the car to become unstable.
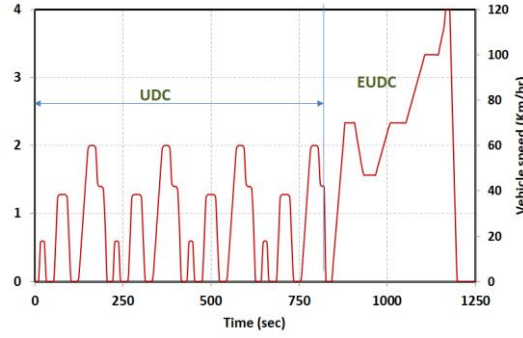
Figure 10: Vehicle speed curve.
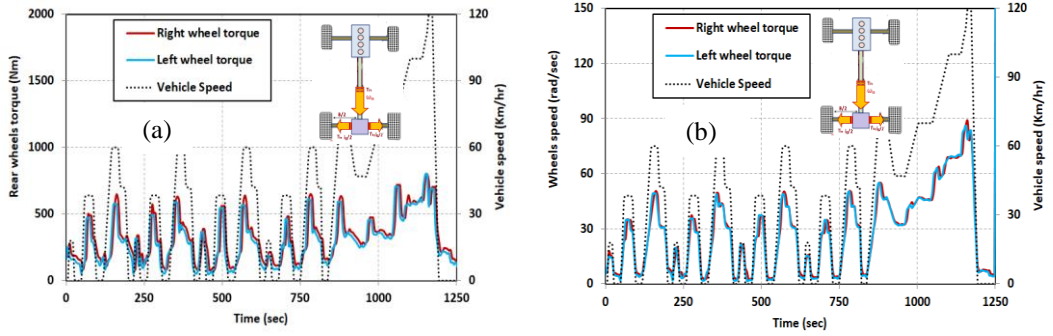
Figure 11: Vehicle wheels torques and speed.
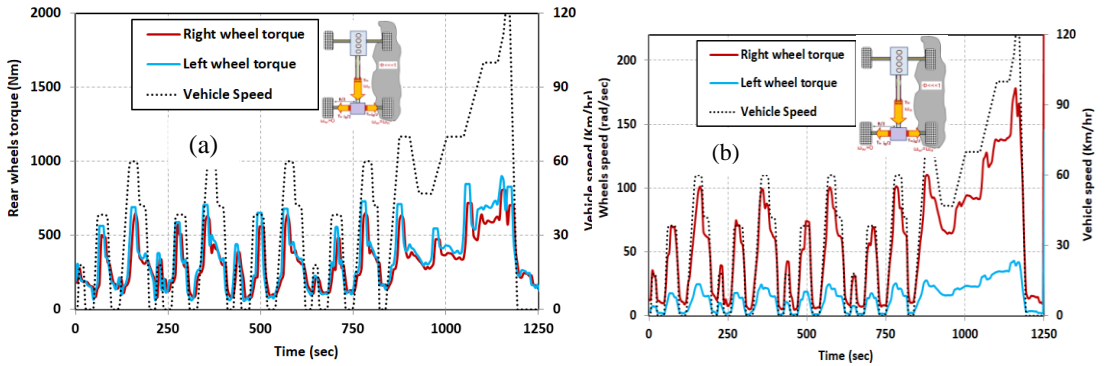
Figure 12: Vehicle wheels torque and speed with the CD with a slippery road.

Figure 13 demonstrates the results of the vehicle wheels torques and speed with the active differential (AD) under a slippery road, the YR and VSS control are applied. When the vehicle right wheels are exposed to a slippery road wet asphalt (μ=0.4) and the left one is exposed to a dry road dry asphalt (Φ=0.8). The AD control avoids the right wheels spinning because for over NEDC more torque is delivered to the left wheels. The rotational speed of the right and left wheels is approximated equal, causing the car to become more stable.

Vehicle stability enhancement based on wheels torque distribution control for
an active differential with electromechanical actuators

31
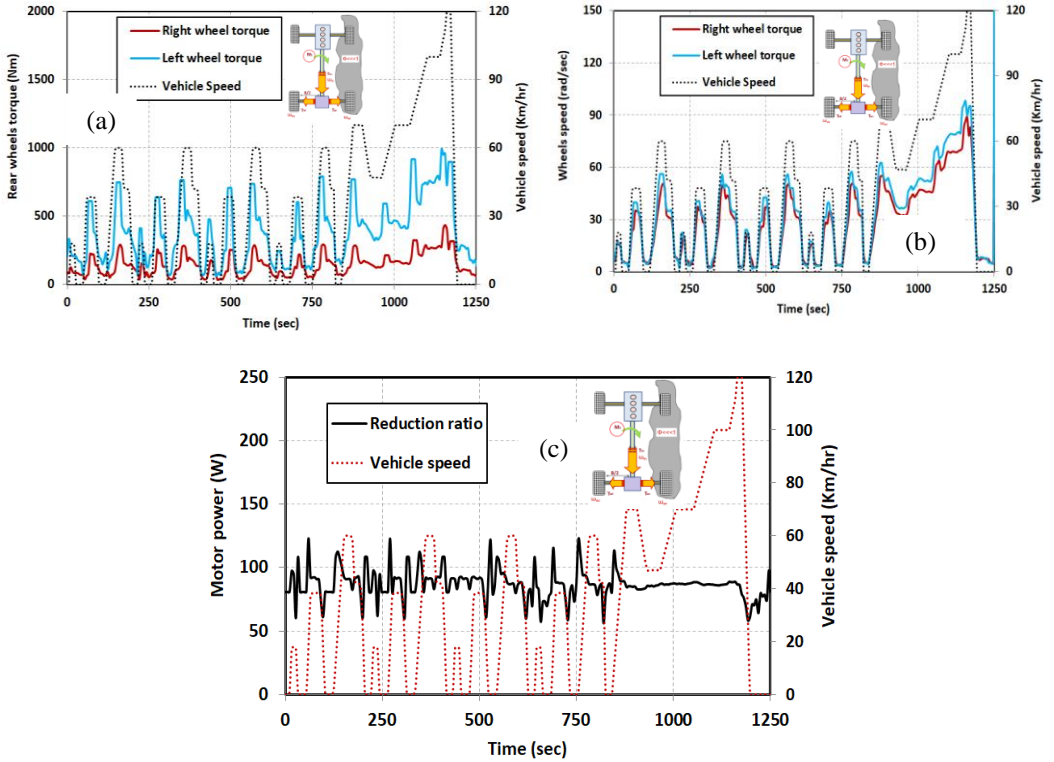
Figure 13: Simulation results of the vehicle wheels torques and speed with the AD with a slippery road.

3.2 Vehicle motion in a left curve

This section's computer simulations are performed at namely J-turn maneuver with constant speeds, to assess the control systems' performance and demonstrate the enhancements brought about by the suggested LQR approach. The simulations involve an automobile cornering during a path following maneuver on a J-turn at longitudinal steady speed V_x=80Km/hr.

Figure 14 shows the results of vehicle responses for the J-turn manoeuvre under uncontrolled, yaw rate (YR) control and integrated YR and vehicle side slip (VSS) control. Referred the step steer analysis, the simulation's chosen steering wheel input angle is depicted in Figure 14(a) and reflects the worst-case situation during collision avoidance. The motorist rapidly shifted the steering wheel from the forward position to the 55^0 position in two seconds. The test result at a dry asphalt road surface (Φ=0.8). Figure 14(b) displays the YR response with three cases control and uncontrolled, where the parameters of the rise time, overshoot, and settle time are all reasonable and the response curves are within the satisfied area with YR control and VSS control, the maximum overshoot at uncontrolled is approximately 20%. Figure 14(c) displays VSS angle response for three cases with control and uncontrolled, where the overshoot is improved and the steady-state error of the system is eliminated at YR+VSS control. Figure 14(d) shows the vehicle lateral velocity, the lateral acceleration are gained at faster response, thus, the vehicle with integrated YR+ VSS control completes its test cycle more quickly. The vehicle with uncontrolled as becomes unstable

during this maneuver, and its side-slip angle and YR sharply rise. According to simulation results displayed in Figure 14, the integrated controller performs better in terms of vehicle stability in typical scenarios when the uncontrolled vehicle becomes unstable, but at the expense of a minor drop in longitudinal velocity when compared to the AD integrated YR+ VSS controller. Integrated controllers can maintain the vehicle within safe margins. Figure 15 demonstrates of the vehicle yaw moment and AD torque under uncontrolled, YR control and integrated YR+ VSS control. Figure 15 (a) illustrates the yaw moment (M_Z), the integrated YR+ VSS control needs the lowest moment value, it is observed that maximum peak yaw moment are 835, 1210 and 1560 Nm under an integrated YR+ VSS control, YR control and uncontrolled respectively. This alteration results in a positive peak that matches the wheels' speed. Figure 15 (b) illustrates the AD torque (M_{diff}) related Eq. (10), it is observed that maximum peak AD moment are 385 Nm and 405 Nm under YR control and an integrated YR and VSS control respectively. According to the figures, the uncontrolled vehicle exhibits an undesired oscillatory response with an increasing side-slip angle and yaw moment. Because the responses are very oscillatory and do not resolve to steady-state values at a finite time. The vehicle's dynamic behavior poses a risk. When compared to the uncontrolled vehicle, these data also show that the controllers have significantly enhanced the vehicle's dynamics performance.
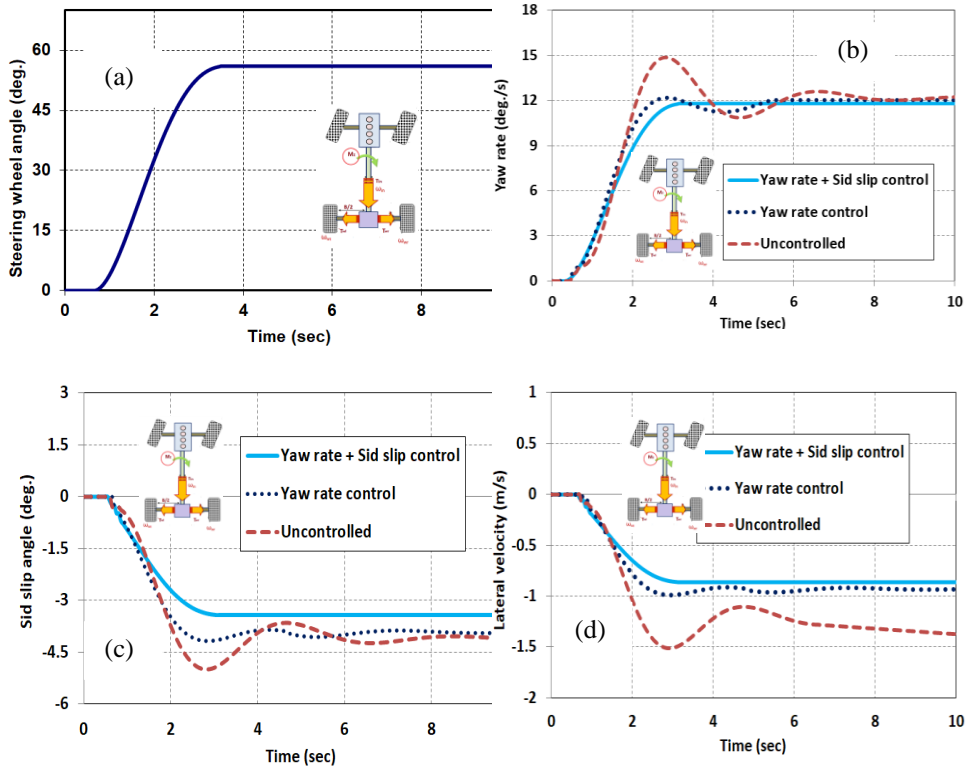
Figure 14: Simulation results of vehicle responses for the J-turn manoeuvre: a. J-turn path input, b. yaw rate, c. side slip angle, d. lateral velocity

Vehicle stability enhancement based on wheels torque distribution control for an active differential with electromechanical actuators

33
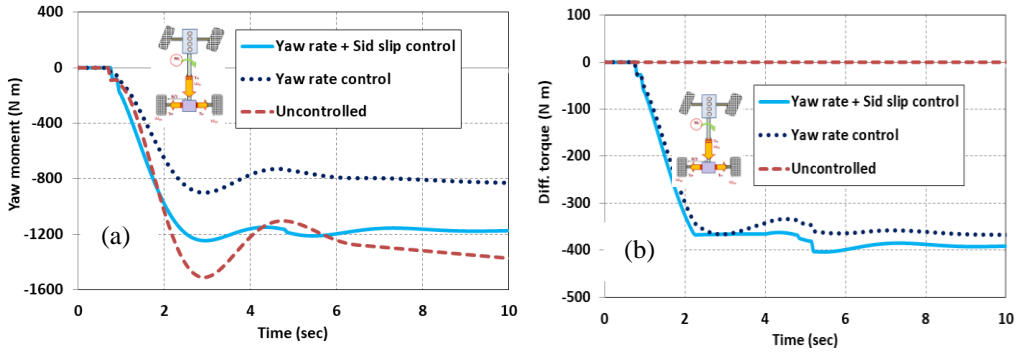
Figure 15: Simulation results with the J-turn manoeuvre: a. yaw moment, b. Active differential torque

Figure 16 and Figure 17 show present the results during the vehicle right wheels are exposed to a slippery road wet asphalt ($\mu=0.4$) and the left one is exposed to a dry road dry asphalt ($\Phi=0.8$), during a path following maneuver on a J-turn at longitudinal steady speed $V_x=80$ Km/hr.

Figure 16 (a) demonstrates the results of yaw moment with a slippery road; the peak value of yaw moment is 900 Nm at the uncontrolled, 785 Nm at the YR control and 620 Nm at the integrated YR+ VSS control. Demonstrate how both YR control and the integrated YR+ VSS control system effectively manage the unstable reaction in the event of uncontrolled. However, the integrated YR+ VSS control system can enhance the vehicle reaction and minimal side distance, which can follow the intended response, in contrast to the case utilizing yaw control. It can be said that the integrated controller uses less effort to accomplish the goals more effectively. Figure 16 (b) demonstrates the results of AD torque with a slippery road, the maximum of AD torque is 420 Nm with an integrated controller and 338 Nm under YR control.

Figure 17 (a) demonstrates the results of the wheels torque with a slippery road, the peak value of wheels moment is 600 Nm for the right wheel under ($\phi=0.8$) and 394 Nm for the left wheel ($\phi=0.4$) with the integrated YR+ VSS control. Figure 17 (b) demonstrates the results of the wheels speed with a slippery road, the peak value of left wheel speed is 68 rad/s for inner wheels, and 62.8 rad/s for the right wheel with the integrated YR+ VSS control, the steady state speed of inner wheels is 40 rad/s and outer side is 58.6 rad/s.
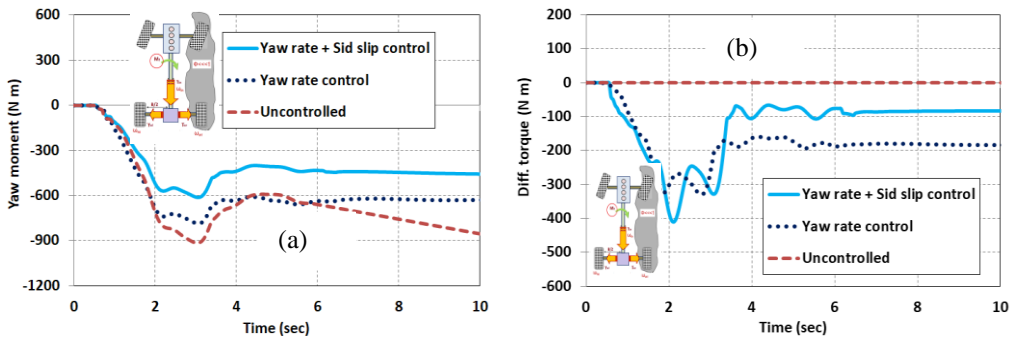
Figure 16: Simulation results with a slippery road: a. yaw moment, b. Active differential
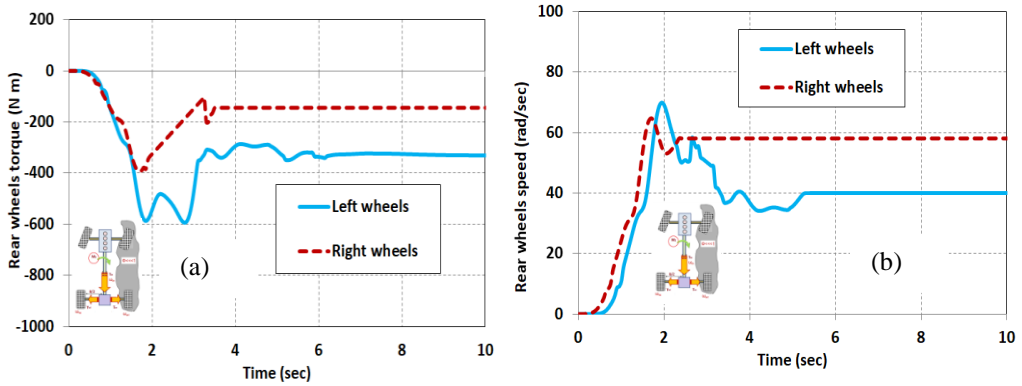
torque

Figure 17: Simulation results with a slippery road: a. wheels torque, b. wheels speed

4   CONCLUSION

This study suggests an active differentials (AD) system with integrated yaw rate (YR) and vehicle side slip (VSS) control to enhance the stability and handling of vehicles. This investigation allows for the deduction of the following conclusions.

- The proposed configuration of the vehicle drive train model with AD is presented, applying the different parameters to the AD mathematical model with two electromechanical actuators.
- The usefulness of the suggested controller is investigated using MATLAB/Simulink in a variety of driving scenarios, including straight lines under NEDC and J-turns with different road adhesions, to regulate lateral slide slip and vehicle YR on different road adhesions can be obtained by an LQR controller.
- The combined control of YR and VSS control is the foundation for an LQR control system for vehicle lateral stability. To produce the corrective yaw moment, a strategy for the AD torque distribution of wheels is designed. The AD torque distribution strategy is developed to generate the corrective yaw moment.
- The peak value of wheel moment is 600 Nm for the right wheel under (ϕ=0.8) and 394 Nm for the left wheel (ϕ=0.4) with the integrated YR and VSS control, it can be said that the integrated controller uses less effort to accomplish the goals more effectively.
- According to simulation results, the vehicle with the suggested AD with a stability control system, which consists of YR and VSS by an LQR, can effectively follow the specified vehicle YR and VSS angle trajectories. It also performs better than the standard Uncontrolled or YR one because YR and VSS lessen the lateral displacement a side force brings.
- The YR undershot and overshot have been somewhat reduced. Additionally, it is anticipated that the vehicle's dynamic reaction and tracking capabilities performance will show promise. The AD with YR and VSS driver assistance system is effective in improving vehicle stability, reducing steering effort, and lane-tracing performance.

REFERENCES

[1] Abe, M., Kano, Y., Suzuki, K., Shibahata, Y., and Furukawa, Y. Side-slip control to stabilize vehicle lateral motion by direct yaw moment. JSAE Rev., 2001, 22(4), 413–419.

[2] E.S. Mohamed, M.I. Khalil and A.A.A. Saad. 2019. Analysis of Synchronous Moment for Active Front Steering and a Two Actuated Wheels of Electric Vehicle Based on Dynamic Stability Enhancement, Int. J. Vehicle Structures & Systems, 11(1), 88-101. doi:10.4273/ijvss.11.1.17.

[3] Shuibo Z. et AL. Controller design for vehicle stability for vehicle stability, Control engineering practical, 14 (2006) 1413-1421.

[4] A.S. Emam and E.S. Mohamed. 2021. Enhancement of Anti-Lock Braking System Performance by using Intelligent Control Technique for Different Road Conditions, Int. J. Vehicle Structures & Systems, 13(1), 37-45. doi:10.4273/ijvss.13.1.09.

[5] Ahmed Shehata Gad, Eid S. Mohamed, and Samir M. El-Demerdash "Effect of Semi-active Suspension Controller Design Using Magnetorheological Fluid Damper on Vehicle Traction Performance' SAE, 2020-01-5101

[6] Baslamisli, S. C., Kose, I. E., and Anlas, G. Gainscheduled integrated active steering and differential control for vehicle handling improvement. Vehicle Syst. Dyn., 2009, 47(1), 99–119.

[7] Eid S. Mohamed, and Saeed A. Albatlan (2014), "Modeling and Experimental Design Approach for Integration of Conventional Power Steering and a Steer-By-Wire System Based on Active Steering Angle Control." American Journal of Vehicle Design, vol. 2, no. 1 (2014): 32-42. doi: 10.12691/ajvd-2- 1-5.

[8] B Mashadi, S Mostaani, M Majidi "Vehicle stability enhancement by using an active differential" Proceedings of the Institution of Mechanical Engineers, Part I: Journal of Systems and Control Engineering 2011, 225: 1098, https://doi: 10.1177/0959651811405113.

[9] Cheli F., et al., A New Control Strategy for A Semi-Active Differential (Part I), 16th IFAC World Congress, 2005

[10] Diachuk, M.; Easa, S.M. Improved Mathematical Approach for Modeling Sport Differential Mechanism. Vehicles 2022, 4, 74–99. https://doi.org/10.3390/vehicles4010005

[11] Shibahata Y., Shimada K., Tomari T., Improvement of Vehicle Maneuverability by Direct Yaw Moment Control, Vehicle System Dynamics Vol. 22, 1993

[12] M. Terzo, Employment of Magneto-rheological Semi-active Differential in a Front Wheel Drive Vehicle: Device Modelling and Software Simulations, SAE Technical Papers 2009-24-0130, 2009, http://dx.doi.org/10.4271/2009-24-0130.

[13] A. Lanzotti, et al., Design and development of an automotive magnetorheological semi-active differential, Mechatronics 24 (5) (2014) 426–435.

[14] Antonio L. et al., Design and development of an automotive magnetorheological semi-active differential, Mechatronics 24 (2014) 426–435.

[15] Federico C. et al., A new control strategy for semi-active differential (part I) All rights reserved 16th Triennial World Congress, Prague, Czech Republic, 2005 IFAC.

[16] Behrooz M. et al., Vehicle path following control in the presence of driver inputs, Proc IMechE Part K: J Multi-body Dynamics 227(2) 115–132.

[17] Riccado M et al.,] "Detailed and reduced dynamic models of passive and active limited-slip car differentials" Mathematical and Computer Modelling of Dynamical Systems, 12, No. 4, ust 2006, 347 – 362.

[18] C Ghike, T Shim, and J Asgari "Integrated control of wheel drive–brake torque for vehicle-handling enhancement" Proc. IMechE , Part D: J. Automobile Engineering, 223, 4, 2009, 439-457.

[19] Julio E et al., Mobile robot path tracking using a robust PID controller, Control Engineering Practice 9 (2001) 1209–1214.

DEVELOPMENT OF AN ENERGY-EFFICIENT CONTROL SYSTEM FOR CONNECTED, HIGHLY AUTOMATED VEHICLES

Alexander Koudrin [1], Sergey Shadrin[2]*

RESEARCH ARTICLE

ABSTRACT: One of the world's most significant challenges is the effort to reduce greenhouse gas emissions. One of the primary sources of these emissions is road transport. On the other hand, road freight transport, which represents a huge portion of freight transportation, accounts for a considerable portion of the company's expenditures on fuel. Reducing fuel consumption and, therefore, greenhouse gas emissions, reducing fuel costs and increasing driving range can be achieved by increasing the energy efficiency of the vehicle. The paper presents a mathematical model for the energy-efficient control of connected, highly automated vehicles. The mathematical model incorporates terrain, speed modes, and traffic light schedules. Laboratory tests of the developed mathematical model are carried out on a digital twin of a test road section recreated on the basis of high-precision navigation data and a passenger vehicle with an internal combustion engine. In the laboratory tests, the proposed system is compared with a vehicle being driven on cruise control. The average speed of both vehicles on the selected route is identical. The results of the experimental runs indicate that the proposed mathematical model is 4.5% more efficient than the vehicle operating on cruise control. Further research is planned to adapt the developed model for hybrid and electric propulsion systems and to conduct field tests on unmanned vehicles with internal combustion engine and electric power plant.

KEY WORDS: *Road vehicle, Digital twin, Simulation, Digital terrain model, Fuel consumption, Mathematical model verification, Automobile, Highly automated transport, Autonomous transport, Energy efficiency, Fuel economy, Energy saving, v2x.*

1 Alexander Koudrin, MADI, 64, Leningradsky Prosp., Moscow, 125319, Russia, Advanced Engineering School of Electric Transport, Moscow Polytechnic University,Bolshaya Semyonovskaya Street, 38, 107023 Moscow, Russia, a.koudrin@outlook.com, https://orcid.org/0009-0000-6679-6425
[2] Sergey Shadrin, MADI, 64, Leningradsky Prosp., Moscow, 125319, Russia, Advanced Engineering School of Electric Transport, Moscow Polytechnic University,Bolshaya Semyonovskaya Street, 38, 107023 Moscow, Russia, a.koudrin@outlook.com, https://orcid.org/0000-0002-2606-9984,
*(Corresponding author)

RAZVOJ ENERGETSKI EFIKASNOG UPRAVLJAČKOG SISTEMA ZA UMREŽENA, VISOKO AUTOMATIZOVANA VOZILA

REZIME: Jedan od najznačajnijih svetskih izazova je nastojanje da se smanje emisije gasova staklene bašte. Jedan od primarnih izvora ovih emisija je drumski transport. S druge strane, drumski teretni transport, koji predstavlja veliki deo transporta tereta, čini značajan deo troškova kompanije za gorivo. Smanjenje potrošnje goriva, a samim tim i emisije gasova staklene bašte, smanjenje troškova goriva i povećanje dometa mogu se postići povećanjem energetske efikasnosti vozila. U radu je prikazan matematički model za energetski efikasnu kontrolu povezanih, visoko automatizovanih vozila. Matematički model uključuje teren, režime brzine i raspored semafora. Laboratorijska ispitivanja razvijenog matematičkog modela vrše se na digitalnom dvojniku probne deonice puta rekonstruisanom na osnovu visoko preciznih navigacionih podataka i putničkom vozilu sa motorom sa unutrašnjim sagorevanjem. U laboratorijskim ispitivanjima, predloženi sistem se upoređuje sa vozilom koje se vozi na tempomat. Prosečna brzina oba vozila na izabranoj trasi je identična. Rezultati eksperimentalnih vožnji pokazuju da je predloženi matematički model za 4,5% efikasniji od vozila koje radi na tempomatu. Planirana su dalja istraživanja radi prilagođavanja razvijenog modela za hibridne i električne pogonske sisteme i izvođenje terenskih ispitivanja na bespilotnim vozilima sa motorom sa unutrašnjim sagorevanjem i elektroenergetskom postrojenjem.

KLJUČNE REČI: *Drumsko vozilo, Digitalni blizanac, Simulacija, Digitalni model terena, Potrošnja goriva, Verifikacija matematičkog modela, Automobil, Visoko automatizovan transport, Autonomni transport, Energetska efikasnost, Ušteda goriva, Ušteda energije, v2k.*

DEVELOPMENT OF AN ENERGY-EFFICIENT CONTROL SYSTEM FOR CONNECTED, HIGHLY AUTOMATED VEHICLES

Alexander Koudrin, Sergey Shadrin

INTRODUCTION

Generally, the factors affecting fuel consumption include many aspects such as vehicle characteristics (e.g., weight, load, engine type, and power consumption of on-board devices), road conditions (e.g., road surface roughness, road gradient, and geometry), and environment (e.g., weather, temperature, and traffic conditions). In addition to these factors, optimizing the driving behavior of human-driven vehicles is considered by many researchers as the main measure used to reduce fuel consumption, this measure has been called "eco-driving". Fuel consumption (l/100 km) varies significantly depending on the speed range. Licheng Zhang et al. [1] developed a new computational approach to accurately estimate the fuel consumption of heavy-duty vehicles. The researchers derived an equation that confirms the proportionality of fuel consumption to speed fluctuations. The greater the oscillation, the more fuel is required to overcome wind resistance, and the more likely it is to decelerate to ensure safe driving - hence there will be more energy lost due to friction as more additional energy is converted to heat energy. The more instances of deceleration, the more noticeable the stop-and-go factor is when driving the same kilometer, which is why frequent acceleration and braking entail more frictional energy loss

Experimental validation included computer simulations and a road experiment. The simulation was conducted using data recorded from the vehicle. The data was collected using an on-board diagnostic port reader. Parameters such as: speed, instantaneous fuel consumption, crankshaft speed, time, mileage and others were recorded on a laptop. Field experiments were conducted with the autonomous vehicle in two driving modes: autonomous and human driven. The test route covered several road scenarios: urban infrastructure, expressways and rural road. The total length of the route was 160 km. The speed range varied from 0 to 130 km/h

The tests showed that speed fluctuations have a significant effect on fuel consumption. When the vehicle is in deceleration mode, fuel consumption is negligible. During the trip, fuel consumption is mainly in cruising mode and during acceleration. The fuel consumption in acceleration mode is about 2 times higher than in cruising mode.

The experiment with the autonomous vehicle took place in a closed area. The vehicle was equipped with lidar, cameras, DGPS, radars and could operate in both autonomous and manual modes. The test vehicle belongs to automation level 3. The experiment was conducted in manual and autonomous mode at two speeds of 20 and 40 km/h. In the test driver control mode, fuel consumption (l/100 km) increased by 5.6%

Juergen Hauenstein et al. [2] also devoted their paper to vehicle energy efficiency, in their paper the authors investigated the effect of terrain on fuel consumption of heavy-duty vehicles. Many truck manufacturers offer on-board systems, which are also called GPS cruise control and are offered by most European manufacturers under brand names, e.g. EfficientCruise from MAN, Predictive Powertrain Control from Daimler, Opticruise from Scania. With topology information via a digital map and current position, energy-efficient rolling maneuvers can be performed. Such driver cues can save up to 7% fuel, but there is a nuance. A study by Samaras et al. found that at very high traffic densities, eco-driving leads to increased fuel consumption rather than fuel savings. Also, eco-driving cars may interfere

with other road users, but it is not clear when this happens and how it can be formalized. Thus, the authors tried to address the problem of energy efficiency in mixed traffic flow.

Collision avoidance takes place using the calculated trajectories of the autonomous vehicle and the planned and desired trajectories of other road users. Due to inaccuracies, e.g. in the collection of measurement data or in the determination of the position or trajectory, a multi-stage collision check is performed. Trajectories are assigned tolerances. At any point in the trajectory, the position may deviate by a previously defined amount. If the selected trajectory is likely to lead to a collision, it is immediately discarded. The trajectories are then evaluated in terms of potential energy costs.

To test the developed system, a route with an uphill gradient of 2% and a downhill gradient of 6% was created. It is assumed that on a 2% gradient a 40 t truck is still able to maintain the maximum allowed speed, in the experiment this speed was 80 km/h. Scenario 1 simulates vehicles other than V2X that are not driven in an energy efficient manner. Scenario 2 represents vehicles other than V2X that are driven in an energy efficient manner, unlike scenario 1. Scenarios 3 and 4 represent V2X vehicles that use joint prediction but do not coordinate maneuvers among themselves. Scenario 3, unlike scenario 4, does not use an energy efficient driving strategy. Scenario 5 presents v2x vehicles that interact with each other and are also equipped with an energy-efficient driving system.

For the two trucks, there was no strong difference between scenarios 2,4 and 5 in terms of fuel economy, with an average fuel economy of 6.56%. In terms of average speed, as expected, scenario 3 took the lead, the other scenarios were between 0.25 and 0.49 meters per second. Scenario 5 was the most energy efficient scenario for the three trucks, with an average fuel saving of 5.61% over the 1500 meter distance. At the same time, the difference in average speed between Scenario 3 and 5 was reduced from 0.26 to 0.2 m/s.

As noted by the authors of the previous paper, the development of 5G technologies will significantly increase the data exchange between vehicles and the surrounding infrastructure. Yasutaka Okada et al [3] developed a system to reduce the fuel consumption of a hybrid vehicle.

In the case of two vehicles, it was found that it is efficient in terms of fuel economy to maintain a driving speed equivalent to the vehicle ahead. At the moment when the driving speed is approaching the speed limit or the distance to the nearest traffic light is short, then it is more efficient to use a different behavior model.

If the vehicle ahead of you starts to slow down or plans to stop before a red traffic signal, it will be ineffective to reduce your speed in the same way as the vehicle ahead. In this case, it is necessary to be able to predict the behavior of the road user ahead. This will allow you to start slowing down in advance and avoid sudden braking.

In the case when the vehicle in front is moving at the maximum permitted speed, the authors propose to introduce a correction in the form of 0.36 km/h to avoid violation. Reducing the maximum permitted speed by this amount will avoid the violation and avoid unnecessary corrections in acceleration/deceleration.

According to the experimental results, it was found that the developed system allows the powertrain to be driven in high efficiency areas and efficiently recover energy. Thus, compared to a transmission with a constant torque ratio, the difference in fuel economy was about 30%.

Bin Zhao et al [4] examined the effect of different scenarios of higher density mixed traffic

flow on vehicle fuel consumption. The mixed traffic flow was modeled on 3 separate road sections: a straight road with one of the lanes reduced, a freeway with gradients, an exit and abutment, and a regulated intersection.

Having analyzed the simulation results, it turned out that in the case with the reduction of one of the lanes, the dependence of fuel economy on the percentage of connected vehicles is approximately linear and at 100% automation of traffic flow reaches 13.7%. In the case of highway traffic it was possible to achieve a significant increase in fuel economy only at 100% automation of the traffic flow, the value was 7.2%. In the scenario with a controlled intersection, approximately the same dependence as in the first scenario was observed, but the effect of the introduction of connected vehicles was more significant - at the level of traffic flow automation of 50% the fuel economy was 19.3%, and at full automation - 40.9%.

Another area for improving the energy efficiency of a vehicle is the management of power distribution to the drive wheels [5,6]. This work examines the factors affecting the efficiency of a multi-purpose wheeled vehicle, focusing on the maximum and average technical speeds. It explains how power-to-weight ratios and suspension parameters determine these speeds and how increasing power-to-weight and mass ratios can result in lower speed gains. The author also discusses various ways of distributing power to the driving wheels of a vehicle, such as disconnecting drive axles and locking differentials. Ways of upgrading the drivetrain of multi-purpose wheeled vehicles to improve efficiency are suggested, including the introduction of four-wheel drive and tyre pressure adjustment.

The utilization of sound source arrival direction estimation technology has the potential to enhance a vehicle's energy efficiency by optimizing its capacity to perceive and navigate its surrounding environment [7]. By accurately estimating the direction of sound sources, an autonomous driving system can enhance its comprehension of the surrounding environment, thereby enabling more informed decision-making about its driving. This may result in a reduction of unnecessary accelerations and decelerations, which are a source of energy wastage. Furthermore, the incorporation of auditory information into the vehicle's sensory systems enables more efficient operation in complex urban environments, facilitating the avoidance of obstacles and the optimization of routes to reduce fuel consumption.

The article is organized as described below. In Approach, we introduce an approach for fuel (energy) saving on hilly roads, including traffic lights and in the field of fuel consumption analysis and optimisation. In Simulation and results, we provide a description of the computer simulation represents results of fuel values for gasoline vehicles with and without use of the proposed algorithm of intelligent speed adjustment.

1   APPROACH

The analysis of scientific solutions for energy efficiency of highly automated vehicles found that:

- Existing scientific studies address disparate energy efficiency problems. Different works consider the energy efficiency of a certain vehicle with a certain type of power plant in certain driving modes.
- Most of the published studies are theoretical in nature, unsupported by experimentation, and need to be proven in the real world.
- Work is needed to develop a comprehensive approach to the energy efficiency of connected, highly automated vehicles regardless of their powertrain, modes and operating conditions. In addition to the scientific novelty justified in the article, the development of such a system has obvious practical significance due to the

economic potential of reducing the costs of transport and logistics companies for passenger and freight transportation by road, and will also reduce the volume of exhaust emissions from highly automated vehicles.

This paper proposes a system adapted for internal combustion engines, taking into account traffic lights and road topography. It will be further developed to meet the above criteria.

1.1 Fuel consumption model

In the present work, the main equation, which is used for calculation of fuel consumption and optimization of control actions, is formula (1) [5].

$$G_t = \frac{\int \frac{3600 \cdot \rho_k \cdot \eta_v}{p_e \cdot \alpha \cdot l_0} \cdot v \cdot (P_r + P_a + P_i + \text{Br}) \cdot \frac{1}{\eta_T} \cdot dt}{\int 755 \cdot v \cdot dt}, \tag{1}$$

where: G_t – fuel consumption per unit of traveled distance, ρ_k – charge density, η – transmission efficiency, η_v – fill factor, p_e – average effective pressure, α – excess air factor, l_0 – theoretically required amount of air for combustion of 1 kg of fuel, v – vehicle speed, Br – braking resistance, t – time, P_a – air resistance, P_i – inertia forces.

The model that takes into account the physics of the car and engine, tested in the article [6], was taken as a basis. The proposed model, in comparison with the previous one, additionally takes into account the following factors (2, 3, 4) [5, 7]:

$$\rho_k = \frac{\rho_0 \cdot 10^6}{R \cdot T_0}, \tag{2}$$

where: R – specific gas constant, ρ_0 – ambient pressure, T_0 – ambient temperature.

$$p_e = p_i - (0{,}089 + 0{,}0118 \cdot \frac{S * n}{30}), \tag{3}$$

where: S – piston stroke, n – crankshaft revolutions, p_i – average indicator pressure.

$$P_r = sin\alpha \cdot g \cdot G + G \cdot g \cdot cos\alpha \cdot \frac{k}{1000} \cdot (5{,}1 + \frac{550000 + 90 \cdot G_k}{P_{TP}} + \frac{1100 + 0{,}0388 \cdot G_k}{P_{TP}} V^2), \tag{4}$$

where: k – coefficient accounting for tire structure; G_k – vertical wheel load; P_{TP} – tire pressure; V – vehicle speed, g – free fall acceleration, α – longitudinal slope of roadway profile, G – vehicle weight

The general view of the implementation of the mathematical model in Matlab Simulink environment is shown in Figure 1.
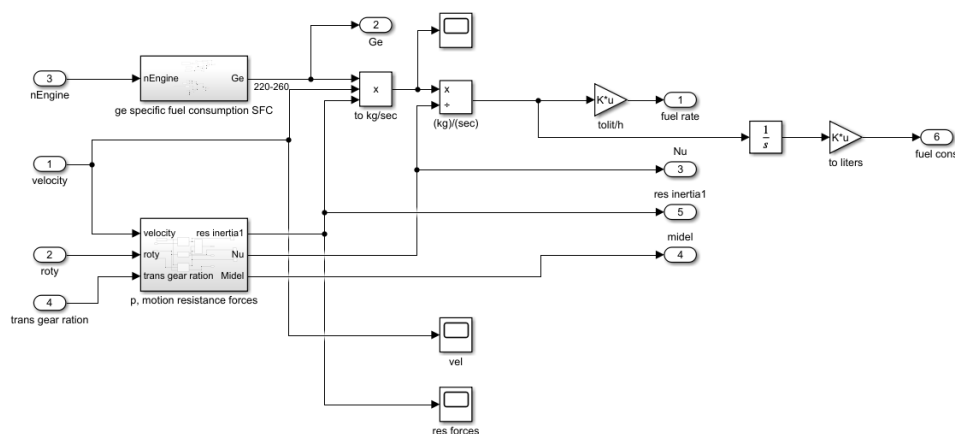
Figure 1 General view of realization of the mathematical model of car fuel consumption in Matlab Simulink environment.

1.2   Method

The output value at the accelerator pedal depends on the following factors: the mode of the nearest traffic light, the predicted road slope, the vehicle acceleration error, the vehicle speed error, the distance to the nearest traffic light, the time to change the speed limit, and the difference between the current speed limit and the future speed limit. Schematic of the proposed method in the Figure 2.
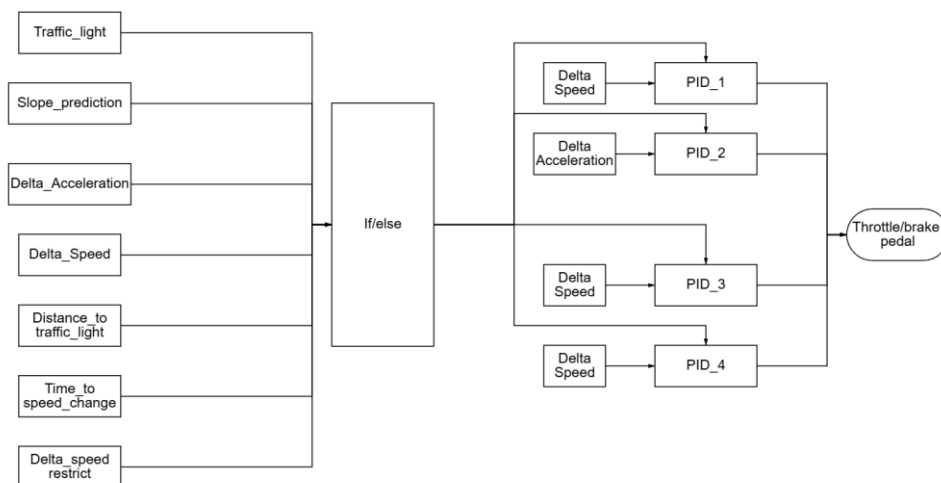
Figure 2 Schematic of the proposed method

Then, depending on the driving conditions, one of the 4 PID controllers is activated. PID_1 - responsible for driving the vehicle on a horizontal road with small deviations from the nominal speed. PID_2 - Responsible for rolling before a speed change and/or traffic light. PID_3 - Responsible for controlling vehicle speed on uphill and downhill slopes. PID_4 - Involved in the driving process if none of the above conditions are met.

There are essentially 2 ways to implement V2X: via cellular links or ad hoc networks. Ad

hoc networks, such as ITS-G5 or IEEE 802.11p, do not require any other infrastructure and send messages via broadcast to all surrounding participants. In cellular networks, such as V2X-LTE or 5G NR mode 1, messages are sent through a cell tower. Cellular networks have the advantage of theoretically infinite range and can handle more data traffic, but only where there is network coverage. In addition to packet loss, there is a delay in receiving messages. On average, this delay is between 90 and 125 ms for IEEE 802.11p and typically more than 2500 ms for V2X-LTE. However, the introduction of 5G in cellular networks is expected to bring significant improvements over LTE technology and reduce latency from 4 to 1 ms. [8].

Within the present work, wireless information exchange between cars and traffic lights was not implemented. The information about the operation mode of the traffic light was received by the automobile instantly. Each traffic light had its own GPS coordinates. The automobile was oriented to the operation of the nearest traffic light. The operation of the traffic light in the Simulink is shown in the figure 3.

Figure 3 Implementation of traffic light in Matlab Simulink

There are 5 traffic lights along the route. Each of the traffic lights has its own operating schedule. The time of red and green light switching on is determined randomly within a specified range. The range of green or red light activation is set via Random source and Switch block.

2   SIMULATION AND RESULTS

To achieve the objectives, computer simulation and full-scale experiment were carried out.

Computer simulation was carried out on a digital twin of the real road, Figure 3, taking into account the elevation difference and traffic light regulation. The characteristics of the route are given in Table 1. The route includes highway and urban roads, with permitted speed limits ranging from 40 to 80 km/h, and 5 intersections with traffic lights and 3 ramps along the way. To create the most accurate virtual copy of the test route, a multi-band RTK GNSS module was used for accurate navigation and mapping [9]. The digital twin was created with mapping requirements in mind [10].
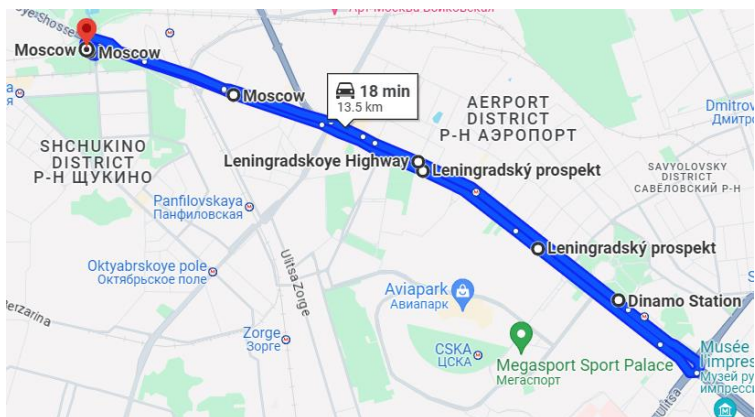
Figure 3 The plot of a real road from which was made the digital terrain model

Table 1. Travel route characteristics

Characteristics	Value
Length, km	13,5
Route type	Closed
Average gradient, %	+- 1
Maximum ascent, %	~ 14
Maximum descent, %	~ 17
Type of pavement	Asphalt concrete
Surface condition	Clean

The test object was a car of category M1 - Chevrolet Orlando I, technical characteristics of which are given in Table 1 [11].

Table 1 Technical characteristics of the experimental car Chevrolet Orlando I

Parameter	Value
Engine	
Engine type	Petrol
Arrangement	Front, lateral
Number of valves per cylinder	4
Cylinder diameter, mm	80.5
Piston stroke, mm	88.2
Compression ratio	10.5
Toxicity standard	Euro 5
Fuel tank capacity, l	64
Powertrain	
Transmission	Automatic
Wheel Drive	Front

The following assumptions were used during simulation:

- the reduction of vehicle speed during maneuvering is not taken into account;
- the traction properties of the wheels and the road surface are unchanged;
- weather conditions (temperature, humidity, air pressure, wind speed) are set to be stable.

The experiment lasted 13.5 kilometers on the entire route and we compared two driving

modes: 1) driving with intelligent speed control with a speed regulation algorithm at a nominal value of speed limit ± 10 km/h, depending on whether the route has an upward or downward slope and taking into account traffic lights; 2) driving with a constant velocity as the average velocity in the first case (and therefore the same time of driving). The results of the experimental run are shown in Figure 4.
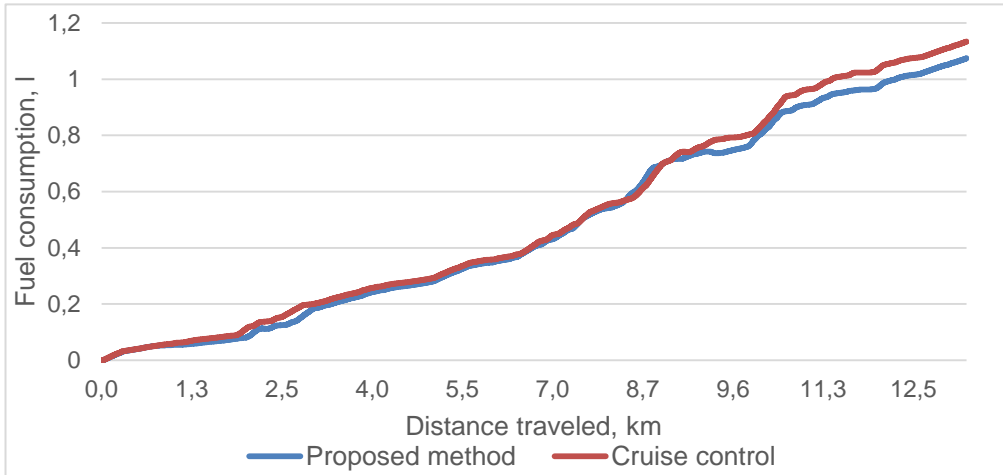

Figure 4 Comparison of fuel consumption with the proposed method and cruise control.

For a vehicle weight of 1650 kg and an average speed of 50 km/h. To draw conclusions from this experiment we will use Figures 5 and 6 for convenience.
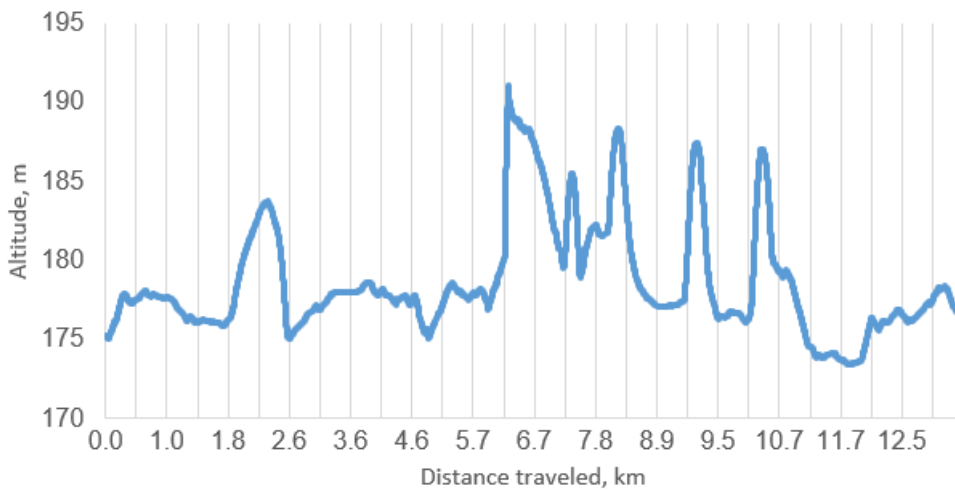

Figure 5 Federal highway altitudes (Leningradsky Prospekt - Volokolamskoye Highway)
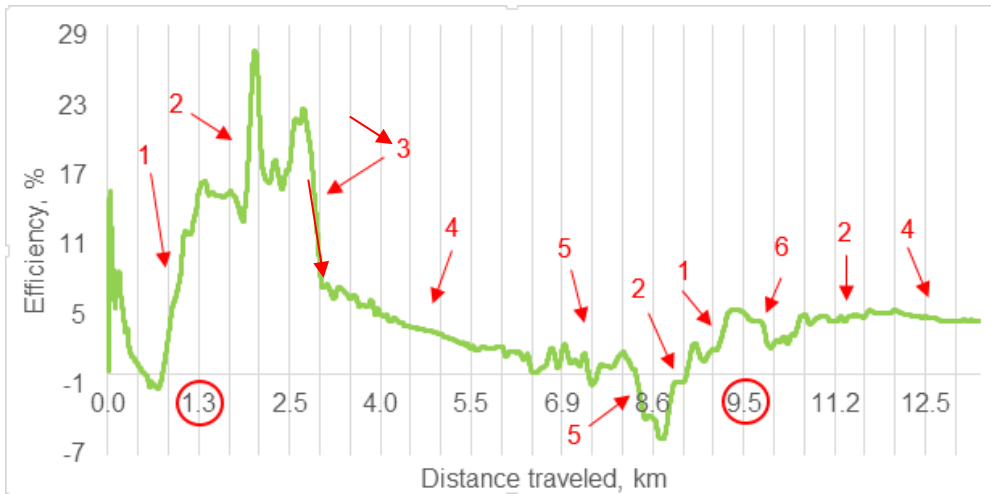
Figure 6 Federal highway altitudes (Leningradsky Prospekt - Volokolamskoye Highway)

The initial velocity of the car was equal to 5 m/s. The operation modes of the traffic lights were regulated randomly by the algorithm described above. In the presented experiment, in the course of the car movement, the red traffic signal was turned on at 2 traffic lights out of 5. The distance at which these traffic lights are located is circled in red in Figure 6. The following conclusions can be drawn as a result of the conducted experiment:

1) Energy efficiency improvement due to topography. Improving energy efficiency by controlling vehicle inertia on hilly terrain is not new. This approach has been successfully used by professional drivers, and it has also been proven to work in highly automated transport studies [12,13].

The proposed method also demonstrates energy efficiency in hilly terrain. This can be seen under figures 2. On the first flyover, the efficiency gain was 15%, while on the second and third flyovers 10% and 2% respectively.

2) Energy efficiency improvement due to V2I. Unlike the terrain, it is more difficult for the driver to predict the mode of operation of traffic lights and plan his maneuver. But this approach also demonstrates high energy efficiency in the reviewed studies [14,15]. The performance of the traffic light interaction of the proposed method can be observed at 2 locations under numbers 1, +15% and + 4%.

3) Negative energy efficiency on flat terrain. The basis of controlling the inertia of the vehicle on hilly terrain is to control the speed in a certain range (in this experiment around 10 km/h) depending on the angle of ascent/descent. This leads to the fact that on overpasses, the average speed of a car equipped with intelligent speed control will be higher than a car with cruise control. In order for both cars to cover the same distance in the same amount of time, it is necessary to set the cruise control to a slightly lower speed than the smart controller. This leads to the fact that on flat terrain (around 1% in this experiment), the fuel consumption of the cruise control car will in any case be lower than the smart controller, which can be observed under numbers 4 in graph 6. In the first case at a distance of 3 km the energy efficiency was minus 5%, in the second case at a distance of 1 km it was minus 1.7%.

Comparing the graph of terrain and energy efficiency, it can be found that in some places after overpasses (3,5) or traffic lights (6), energy efficiency is not so significant or even negative. Here we can draw another conclusion that was not touched upon in the energy

efficiency studies that I was able to study:

4) Road infrastructure can have a significant impact on vehicle energy efficiency. Vehicle inertia control on hilly terrain is designed to drive up a hill at high speed and then accelerate down the hill. It is easier for the car to move downhill under the influence of gravity than uphill, so the fuel consumption per unit of traveled distance will be less. It is at these moments that the speed of the car is controlled (increasing the speed on the downhill and decreasing it on the uphill). Thus, ideally, nothing should prevent the car from going uphill or downhill. But in reality, this is not always the case. The number 3 on the energy efficiency graph symbolizes the overpass exit shown in Figure 7. The red line in Figure 7 represents the vehicle's trajectory. Ideally, the car should accelerate to 80 km/h from the ramp and save fuel. In reality, it turns out that the car accelerates to about 60, after which it is forced to brake, otherwise it simply will not fit into the realignment across 2 lanes (one of which is a bus lane) at a distance of 100 meters. In medium or dense traffic in this place cars may even stop to make such a maneuver. In the described experiment, by performing this maneuver the energy efficiency was reduced from 23% to 7%.

Figure 7 Exit ramp near Dynamo

The ideal situation for controlling the vehicle's inertia on hilly terrain is when one uphill/downhill section immediately alternates with another, bypassing the flat terrain sections we described in point 3. The road section from kilometer 6 to kilometer 9 is exactly like this. There are 3 overpasses in this distance. But the whole effect of the energy efficient management is offset by the speed limits (number 5 in figure 6). This is especially visible at a distance of 8.5 kilometers. The car accelerates to a speed of 100 km/h when descending from the previous overpass and must reduce its speed to 40 km/h over a distance of 150 meters when entering the next ramp. This is quite intensive braking and all the energy saved goes into heat. As a result, this maneuver resulted in an energy efficiency loss of 7%. Under number 6 is an example of another failed infrastructure solution in terms of vehicle energy efficiency. At a distance of 9.5 kilometers there is a traffic light, which in the presented scenario was red when the car reached it. Figure 5 shows that this traffic light is located directly after the downhill exit from the ramp. In this case we have 2 energy efficiency models overlaid at the same time in the same location. We need to pick up speed while descending from the ramp and we need to roll (which in this case will not give a visible advantage, because the car is moving from the downhill slope and we will have to use brakes anyway) before the traffic light. In the end, neither approach saves fuel and as a result we get

an energy efficiency of -2%. Negative energy efficiency is taken from the point of view that we should have been moving faster on that stretch than we actually did. All our energy has gone into the heat of braking. Yes, the car with cruise control also braked on this section, but it was traveling at a slower average speed on the previous section, hence the -2% difference. This overpass exit is also unfortunate because of its location. We have previously described how a car should ideally behave when descending an overpass. If the green traffic signal was on, the car would accelerate to 60 km/h when going down the overpass, after which it would have to brake to 30 km/h to fit into a turn of more than 90 degrees, figure 8.

Figure 8 Exit ramp near Streshnevo

Of course, all the infrastructure solutions discussed above are made with safety in mind. In this article, these solutions have only been evaluated from the point of view of energy efficiency. Despite the negative factors, the proposed system demonstrates an energy efficiency of 4.5% in mixed conditions.

3   CONCLUSIONS

The developed method demonstrates energy efficiency both on a highway and in an urban area. The algorithms have an integrated approach to energy efficiency: they take into account the terrain of the road and interact with the road infrastructure.

The main results and conclusions of this study are as follows:

- 1. A mathematical model that improves the energy efficiency of connected, highly automated vehicles with internal combustion engines is proposed.
- 2. Virtual tests of the developed algorithms were carried out on a digitized section of a real road, taking into account the height difference, intersections and traffic light regulation.
- 3. Comparison of the results of car fuel consumption modelling with the proposed algorithms and cruise control was carried out. The proposed algorithms showed an efficiency of 4.5 % on a passenger car with internal combustion engine.

Plans for further research:

- 1. Integrate the developed energy efficiency algorithms into a real highly automated vehicle.
- 2. Conduct field tests of the developed algorithms on the road considering elevation

difference, intersections and traffic light regulation.
- 3. Adapt the proposed algorithms to hybrid propulsion and electric traction vehicles.
- 4. Conduct comparative tests of energy efficiency and cruise control algorithms for hybrid and electric propulsion system

FUNDING

REFERENCES

[1] Licheng Zhang,Ting Zhang,Kun Peng,Xiangmo Zhao,and Zhigang Xu Journal of Advanced Transportation – 2022. - Volume 2022, Article ID 2631692, 12 pages (https://doi.org/10.1155/2022/2631692)

[2] Juergen Hauenstein, Jan Cedric Mertens , Frank Diermeyer and Andreas Zimmermann Electronics 2021, 10(19), 2373; (https://doi.org/10.3390/electronics10192373)

[3] Yasutaka Okada1•Shunki Nishii1•Akihiro Takeshita1•Kazuki Harada1•Yudai Yamasaki Control Theory and Technology volume 20, pages197–209 (2022) (DOI:10.1007/s11768-022-00094-y)

[4] Bin Zhao, Yalan Lin, Huijun Hao, and Zhihong Yao Journal of Advanced Transportation Volume 2022, Article ID 6345404, 14 pages (https://doi.org/10.1155/2022/6345404)

[5] Keller, A. and Aliukov, S., "Effectiveness of Methods of Power Distribution in Transmissions of All-Wheel-Drive Trucks," SAE Technical Paper 2015-01-2732, 2015, doi:10.4271/2015-01-2732.

[6] A. Keller, and S. Aliukov, "Analysis of Possible Ways of Power Distribution in an All-wheel Drive Vehicle," Lecture Notes in Engineering and Computer Science: Proceedings of The World Congress on Engineering 2015, 1-3 July, 2015, London, U.K., pp1154-1158.

[7] Y. M. Furletov, A. M. Ivanov, S. S. Shadrin and M. A. Toporkov, "Sound Source Direction of Arrival Estimation for Autonomous Driving Applications," 2022 Intelligent Technologies and Electronic Devices in Vehicle and Road Transport Complex (TIRVED), Moscow, Russian Federation, 2022, pp. 1-5, doi: 10.1109/TIRVED56496.2022.9965523.

[8] Bosch Automotive Handbook 9th Ed. p 1544

[9] Litvinov A.S., Farobin YA. Ye. Car. Theory of operational properties, Moscow, 1989, 240 p.

[10] Krivoshapov S. I. Calculation methods for determining of fuel consumption per hour by transport vehicles / Krivoshapov S. I., Nazarov A. I., Mysiura M. I., Marmut I. A. // IOP Conference Series Materials Science and Engineering – 2020 - 977(1):012004 - DOI:10.1088/1757-899X/977/1/012004

[11] Koudrin A. B., Shadrin S. S. Bulletin of the Moscow Automobile and Road State Technical University (MADI) – 2023, № 2(73), pages 15-22.

[12] [Technical characteristics of measuring equipment]. Available at: https://emlid.com/reach/?ysclid=llzeqysm 89780605720 (accessed 20 July 2024).

[13] Komissarova T.S., Petrov D.V. [Cartography: textbook. (section C)]. Saint Petersburg, LGU im. A.S. Pushkina Publ., 2010. 212 p.

[14] Car specs database, auto-data.net, https://www.auto-data.net/en/chevrolet-orlando-i-1.8-16v-141hp-16939

[15] Zavalko, A. Applying energy approach in the evaluation of eco-driving skill and eco-driving training of truck drivers. Transp. Res.Part D Transp. Environ. 2018,62, 672–684

[16] Sciarretta, A.; Vahidi, A. Energy-Efficient Driving of Road Vehicles; Springer International Publishing: Cham, Switzerland, 2020;ISBN 978-3-030-24126-1

[17] Z. Xu, Y. Wang, G. Wang et al., "Trajectory optimization for aconnected automated traffic stream: comparison between anexact model and fast heuristics," IEEE Transactions on In-telligent Transportation Systems, vol. 22, no. 5, pp. 2969–2978,2021

[18] M. H. Almannaa, H. Chen, H. A. Rakha, A. Loulizi, and I. El-Shawarby, "Reducing vehicle fuel consumption and delay at signalized intersections: controlled-field evaluation of eff ec-tiveness of infrastructure-to-vehicle communication,"Transportation Research Record: Journal of the TransportationResearch Board, vol. 2621, no. 1, pp. 10–20, 2017.

Intentionally blank

THE MODERN APPROACH TO PROBLEM-SOLVING IN MECHANICAL ENGINEERING - APPLICATION OF ARTIFICIAL INTELLIGENCE

Igor Saveljić [1], Slavica Mačužić Saveljić [2], Nenad Filipović [3]*

RESEARCH ARTICLE

ABSTRACT: This study explores the integration of artificial intelligence (AI) as a contemporary problem-solving approach in mechanical engineering. Beginning with an overview of artificial intelligence, the paper delves into its applications within various industries, focusing on its impact. By drawing insights from recent literature, the study examines how AI technologies have reshaped problem-solving methodologies. Through a detailed exploration of current studies and advancements, the research highlights AI's role in enhancing efficiency, precision, and innovation in processes. Ultimately, the paper aims to provide a comprehensive understanding of artificial intelligence's significance in modern problem-solving strategies employed within the mechanical engineering domain.

KEY WORDS: *Artificial intelligence, efficiency, mechanical engineering, research*

[1] *Igor Saveljić, Institute for Information Technologies, University of Kragujevac, bb Jovana Cvijića Str., 34000 Kragujevac, Serbia, isaveljic@kg.ac.rs, https://orcid.org/0000-0002-0707-5174,(*Coorresponduing author)*
2 Slavica Mačužić Saveljić, University of Kragujevac, Faculty of Engineering, 6 Sestre Janjić Str., 34000 Kragujevac, Serbia, s.macuzic@kg.ac.rs, https://orcid.org/0000-0003-2635-2496
3 Nenad Filipović, University of Kragujevac, Faculty of Engineering, 6 Sestre Janjić Str., 34000 Kragujevac, Serbia, fica@kg.ac.rs, https://orcid.org/0000-0001-9964-5615

SAVREMENI PRISTUP REŠAVANJU PROBLEMA U MAŠINSTVU - PRIMENA VEŠTAČKE INTELIGENCIJE

REZIME: Ova studija istražuje integraciju veštačke inteligencije (AI) kao savremenog pristupa rešavanju problema u mašinstvu. Počevši od pregleda veštačke inteligencije, rad se bavi njenim primenama u različitim industrijama, fokusirajući se na njen uticaj. Izvlačenjem uvida iz novije literature, studija ispituje kako su AI tehnologije preoblikovale metodologije rešavanja problema. Kroz detaljno istraživanje trenutnih studija i napretka, istraživanje naglašava ulogu veštačke inteligencije u poboljšanju efikasnosti, preciznosti i inovacija u procesima. Na kraju, ovaj rad ima za cilj da pruži sveobuhvatno razumevanje značaja veštačke inteligencije u savremenim strategijama rešavanja problema koje se koriste u domenu mašinstva.

KLJUČNE REČI: *Veštačka inteligencija, efikasnost, mašinstvo, istraživanje*

THE MODERN APPROACH TO PROBLEM-SOLVING IN MECHANICAL ENGINEERING - APPLICATION OF ARTIFICIAL INTELLIGENCE

Igor Saveljić, Slavica Mačužić Saveljić, Nenad Filipović

INTRODUCTION

Artificial Intelligence represents a growing scientific discipline that explores and develops the theory, technology, and application systems for simulating and extending human intelligence, including disciplines such as psychology, cognitive sciences, science of thinking, computer science, system science, and biosciences [1]. Artificial Intelligence essentially simulates the process of human thought data interaction with the hope of understanding the essence of human intelligence and then producing a smart machine. This intelligent machine can react and solve problems in a similar way to a human being [2], [3].

With the continuous advancement of science and technology, mechanical engineering is also constantly evolving and changing, moving from traditional mechanical engineering to electromechanical engineering. Its level of automation and intellectualization is continuously improving, entering a new stage of development [4].

The application of AI technology is based on the assumption of computer technology development, which has improved computer technology through its analysis to achieve the realization of intelligent technology. When intelligent technology is applied in mechanical engineering, it mainly achieves the automation of mechanical engineering control [5], [6]. The applications of artificial intelligence in mechanical engineering are not just the use of computer technology, but also the combination with information technology, psychology, linguistics, and other areas of knowledge.

The aim of this paper is to report on the composition and development of AI, as well as the relationship between artificial intelligence and mechanical engineering. Most importantly, the goal is to explore how artificial intelligence is applied in the field of mechanical engineering.

1 ARTIFICIAL INTELLIGENCE IN MECHANICAL ENGINEERING AND AUTOMOTIVE INDUSTRY

In the modern era, the application of artificial intelligence and machine learning (ML) in mechanical engineering and the automotive industry is becoming increasingly significant due to the potential this technology offers in optimizing problem-solving, improving design processes, and enhancing production efficiency. Subsequently, there will be a review of contemporary literature in this field to further explore current studies, advancements, and applications of artificial intelligence in these areas.

Research [7] delves into the realm of smart computer programs that possess the ability to learn independently, showcasing their potential in enhancing machine design. It expounds on the fundamental aspects of these intelligent programs, juxtaposing various types and shedding light on the tools and data utilized by engineers in this domain. Global research examples demonstrate the current efficacy of these programs in the realm of machine part design. Despite the potential for high costs and time-intensive processes in optimizing these intelligent programs, the paper underscores the evolving landscape towards increased efficiency and affordability. To propel further advancements, the paper concludes by

proposing areas for researchers to explore, aiming to continually refine the application of smart programs in the realm of machine design.

Authors [8] explore into the impact of new computer technologies on China's machine-making industry, emphasizing its growth and enhanced efficiency. It elucidates the role of these technologies under the umbrella term of AI, likening it to empowering computers to think autonomously and learn tasks independently. Furthermore, the study underscores the advantageous effects of implementing artificial intelligence in optimizing the performance of machines, thereby boosting productivity and positively impacting the economy. As countries worldwide focus on harnessing these technologies to maintain competitiveness in production, it becomes evident that the integration of traditional machine-making practices with contemporary computer technologies holds significant promise. In its closing remarks, the paper advocates for further exploration and research on how artificial intelligence can continuously elevate the machinery industry, showcasing a path towards ongoing enhancement and innovation.

Artificial intelligence, a sophisticated form of computer technology, is increasingly integrated into the manufacturing process, aiding in the identification of flaws, quality checks, and enhancing workplace safety standards [9]. This innovative technology has seamlessly integrated itself into daily life, evident in the prevalence of smart appliances like dishwashers and sweepers, showcasing its fusion with machine production. Its crucial role lies in ensuring precise manufacturing standards, consequently improving work efficiency and ensuring the safety of individuals. The advent of artificial intelligence is ushering in a transformative wave in the machine-making industry, facilitating automation and smarter functioning in factory settings. By leveraging artificial intelligence, individuals can streamline the process of sourcing required machine parts through image recognition or computer models, alleviating the need for memorizing intricate technical details.

The special issue of the journal [10] presents 10 new studies focusing on the practical applications of AI in various aspects of manufacturing processes. These studies showcase how AI plays a crucial role in optimizing manufacturing operations, from machine maintenance and production planning to intricate tasks such as laser metal shaping, plastic component integration, and complex assembly procedures. The research emphasizes how AI technology enhances efficiency, problem-solving capabilities, and overall productivity in manufacturing settings.

Group of authors [11] reviewed how AI, especially artificial neural networks (ANNs), is used for checking machine health, analyzing machine parts, and improving designs. It's still early days for using ANNs in this way, but they're already showing they can make systems more efficient. The paper also talks about a special kind of AI network that helps identify problems in machines that move back and forth really fast. This AI network uses sound, oil, and other signals to figure out what's wrong with the machines. The research is important because it can help factories and businesses save money by catching problems early.

Investigation [12] demonstrates how AI has been used in engineering over the last five years, focusing on things like learning from data, making smart choices, and improving designs. Researchers are paying more attention to AI that can explain how it makes decisions, and they're finding that AI can do things faster and more accurately than humans in some cases. It's important to pick the right kind of AI for each engineering problem to get the best results.

Author [13] reports how AI can plan the best path for a robotic arm to move, using a method called the ant colony algorithm. The ant colony algorithm is inspired by how real ants find

the shortest path to food, but the paper talks about making this method even better. By improving the ant colony algorithm, the robotic arm can work faster and more efficiently, which is great for businesses that use these machines. The paper tested the new method and found that it was indeed better than the original, making it a promising tool for future mechanical engineering projects.

Mechanical engineers design machines, and now they're using AI, which is like a smart computer helper, to make better designs [14]. AI has been around since 1956 and is really good at tasks like planning how parts move and figuring out forces in machines. Sometimes machines are too complicated, and that's when AI becomes super useful for mechanical engineers. The paper shows how AI and mechanical engineering are starting to work together, which is a new kind of teamwork between computer and mechanical engineers. There are examples in the paper of how AI has helped in designing machines, which might inspire more cool projects.

The next research [15] explores how smart computer programs are used to make the process of designing gear-reducing machines more efficient. It discusses the challenge of using the internet to quickly access and share design tools, data, and knowledge for creating these machines. A new AI algorithm, which is a set of rules for the computer to follow, is introduced to improve the design process. The paper also talks about using a neural network model, which is a computer system designed to think like a human brain, to make the design system stronger. Finally, the research includes tests to show how these AI methods can make the manufacturing of gear-reducing machines better.

The study [16] discusses how to use computer programs to make designing parts for machines easier and better by using AI, which is like a smart helper that can think and learn. It talks about the problem of getting and sharing design tools and information over the internet quickly and easily. The paper introduces a new smart AI method to improve how machines are designed. To make the design system more reliable, it uses a special kind of AI that works like the human brain. The research also includes tests to show that these AI methods can improve the making of machines.

The paper [17] discusses the importance of AI, focusing on three main AI technologies: physical robot technology, machine learning, and RPA (Robotic Process Automation). Physical robots, which are a crucial part of AI development, are changing various industries by performing tasks that humans used to do. Machine learning, a type of AI that allows machines to learn from experience, is used to make better decisions in mechanical and electronic engineering. RPA is a technology that automates repetitive tasks, which helps in making the manufacturing process more efficient and of higher quality.

In the last 20 years, this technology has helped many parts of life and work, like business and space, and has made things better and more efficient. The paper [18] talks about how artificial intelligence is now playing a big role in mechanical engineering, helping to solve problems and improve experiments and the way machines are made (Figure 1). By using advanced technology and smart computer programs, artificial intelligence can find and fix issues in mechanical automation, which is when machines work on their own without people having to control them all the time. The article aims to look closely at how artificial intelligence can be used in the area of making machines work automatically and the benefits it brings.
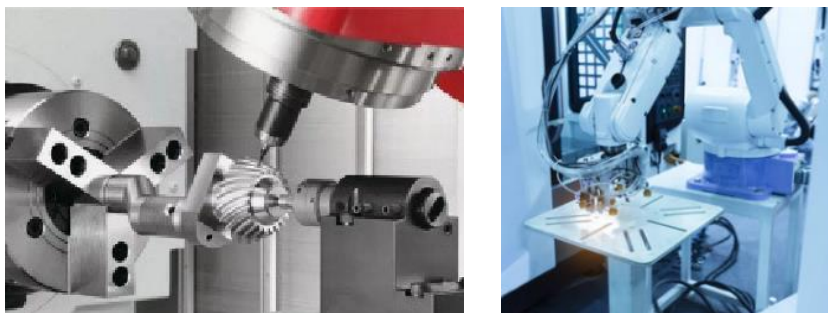
Figure 1 Application of artificial intelligence in mechanical processing [18]

The rapid advancement of AI in the automotive industry is astonishing. Looking ahead, the future of AI in this sector is increasingly intriguing. Projections suggest that by 2033, the market will expand to an impressive $35.71 billion. This surge reflects AI's transformative influence on the automotive sector, highlighting its essential role within the industry [19].

Figure 2 Automotive artificial intelligence market size 2023 (USB Billion) [19]

AI is not only transforming automotive technology on the road, but also reshaping customer experiences. The integration of AI enhances digital car shopping and ownership by making them more user-friendly and engaging. This progression is expected to boost the online car-buying market to $754.2 billion by 2024, highlighting the growing demand for personalized, AI-driven services.

The industry stands on the edge of a major shift as AI integrates data and innovations throughout the automotive spectrum. By 2031, the automotive data analytics market is projected to reach $15,387 million. AI's ability to analyze data transforms decision-making, improves real-time vehicle diagnostics, and changes maintenance and safety practices. AI in the automotive sector is driving a revolution focused on efficiency and safety, enhancing the human experience. Each innovation, from AI-driven design to smart cars, contributes to a vision of the future where technology and transportation seamlessly merge.

According to study [20], AI is poised to transform automobile manufacturing. As AI applications grow, from driver assistance to AI-powered fleet management, companies are revising operations to enhance performance and productivity through AI diagnostics. The current integration of AI in vehicles signals a shift toward self-driving cars becoming standard, with autonomous vehicles projected to comprise 10-15% of new car sales by 2030. AI is not just improving the driving experience; it is redefining the automotive industry, promoting a future of interconnected efficiency, safety, and innovation.

In the provided literature, there is a clear focus on the integration and impact of AI across various fields, including the automotive industry. These discussions highlight the significant potential of AI in enhancing problem-solving capabilities, automation, and efficiency within the engineering domain. Specifically, in the automotive sector, AI is pivotal in developing advanced driver assistance systems and optimizing manufacturing processes to create more efficient vehicles. The papers collectively underscore the transformative role of AI in revolutionizing design processes, improving machine performance, and streamlining manufacturing operations. Additionally, the texts stress the importance of AI in ensuring precise standards, enhancing workplace safety, and accelerating advancements in technological innovations. The studies also showcase how AI is increasingly being adopted in diverse applications, ranging from machine maintenance and part optimization to complex problem-solving tasks. Overall, the papers present a compelling argument for the continued integration and exploration of AI technologies in engineering practices to drive efficiency, productivity, and innovation in the industry.

2   CONCLUSION

The integration of artificial intelligence and machine learning into mechanical engineering offers numerous advantages that significantly enhance various aspects of the field. One of the primary benefits is improved design. AI and ML allow engineers to create more efficient mechanical components and parts by analyzing data from previous projects. This analysis leads to more accurate designs that better meet the specific needs of each project.

Another advantage is automation. AI and ML can automate certain tasks, reducing the time and effort required to complete them and minimizing the possibility of errors. This not only streamlines the workflow but also enhances reliability and precision in executing repetitive tasks.

The implementation of AI and ML also leads to substantial cost savings. By optimizing the design and manufacturing processes, engineers can lower production costs, making projects more cost-effective and reducing overall expenses. This economic efficiency is particularly advantageous in large-scale production environments.

Furthermore, AI and ML significantly increase productivity. Automating routine tasks permits engineers to dedicate more time and effort to complex problems that require innovative and creative thinking. This shift in focus boosts the overall productivity of engineering teams, enabling them to achieve more in less time.

Lastly, the quality of mechanical products is greatly improved through the use of AI and ML. By analyzing data from past projects, engineers can pinpoint areas for improvement and implement changes that enhance the final product's quality. This results in superior mechanical components that meet higher standards of performance and durability.

In summary, the integration of AI and ML in mechanical engineering and automotive industry leads to improved design accuracy, task automation, cost reduction, increased productivity, and higher product quality, collectively advancing the field in notable ways.

ACKNOWLEDGMENTS

REFERENCES

[1]   Liu, J. N.: "Discussion on Relation between Mechanical Electronic Engineering and Artificial Intelligence,"Journal of Tianjin Vocational Institutes, Vol. 20, 2018, pp. 76-79.

[2]   Russell, S., Norvig P.: "Artificial Intelligence: A Modern Approach, "4th ed. Prentice Hall, 2020.

[3]   Wen, W. H.: "Application of artificial intelligence technology in mechanical and electronic engineering, "Automation and instrumentation, Vol. 2, 2016, pp. 96-97.

[4]   Lei, Y., Yang, B., Jiang, X., Jia, F., Li, N., Nandi A. K.: "Applications of machine learning to machine fault diagnosis: A review and roadmap,"Mech. Syst. Signal Process. Vol. 138, 2020.

[5]   Zheng, H., Moosavi, V., Akbarzadeh, M.: "Machine learning assisted evaluations in structural design and construction, "Autom. Constr., Vol. 119, 2020, pp. 103–346.

[6]   Chang, C. W., Lee, H. W., Liu, C. H.: "A Review of Artificial Intelligence Algorithms Used for Smart Machine Tools,"Inventions, Vol. 3, No. 41, 2018.

[7]   Jenis, J., Ondriga, J., Hrček, S., Brumercik, F., Čuchor, M., Sadovsky, E.: "Engineering Applications of Artificial Intelligence in Mechanical Design and Optimization,"Machines, doi: 10.3390/machines11060577, 2023.

[8]   Jiaheng, H.: "The application of artificial intelligence technology in the field of mechanical and electronic engineering reflects, "International Conference on Mathematics, Modeling and Computer Science, doi: 10.1117/12.2671679, 2023.

[9]   Ferit, A.: "Applications of Artificial Intelligence in Mechanical Engineering, "Europan journal of science and technology, doi: 10.31590/ejosat.1224045, 2022.

[10] Keiichi, N., Keigo, T.: "Editorial: Application of Artificial Intelligence Techniques in Production Engineering, "International journal of automation technology, doi: 10.20965/ijat.2023.p0091, 2023.

[11] Alhakeem, M. R. H., Ilham, D. N.: "Application of Artificial Intelligence in Mechanical Engineering, "Brilliance: Research of Artificial Intelligence, Vol. 2, No. 3, 2022, pp. 177-181.

[12] Khaleel, M., Ahmed, A. A., Alsharif, A.: "Artificial Intelligence in Engineering, "Brilliance: Research of Artificial Intelligence, Vol. 3, No. 1, 2023, pp. 32-42.

[13] Chen, Y.: "Relevance Research of Artificial Intelligence Technology in the Field of Mechanical Engineering," 2022 World Automation Congress (WAC), San Antonio, TX, USA, 2022, pp. 453-457.

[14] Arturo, J.: "The Design of Mechanisms via Artificial Intelligence,"   doi: 10.58830/ozgur.pub95.c437, 2023.

[15] Ye, X.: "Application of Computer CAD Software Optimization in the Manufacture of Mechanical Reducer Considering Artificial Intelligence," 2022 International Conference on Edge Computing and Applications (ICECAA), Tamilnadu, India, 2022, pp. 1057-1060.

[16] Xianzhen, Y.: "Application of Computer CAD Software Optimization in the Manufacture of Mechanical Reducer Considering Artificial Intelligence," 2022 International Conference on Edge Computing and Applications, doi: 10.1109/ICECAA55415.2022.9936183, 2022.

[17] Yunze, Y.: "The value and application of artificial intelligence technology in mechanical and electronic engineering," Academic Journal of Engineering and Technology Science, doi: 10.25236/ajets.2022.050702, 2022.

[18] Wanling, L., Fanzhao, M.: "Research on the Application of Artificial Intelligence in the Field of Mechanical Automation," J. Phys.: Conf. Ser. 1885, doi: 10.1088/1742-6596/1885/4/042015, 2021.

[19] https://www.precedenceresearch.com/automotive-artificial-intelligence-market

[20] Breunig, M., Kässer, M., Klein, H., Stein, J.P.:" Building smarter cars with smarter factories: How AI will change the auto business, McKinsey and Company, 2024.

Intentionally blank

THE INFLUENCE OF THERMAL STRESS OF DISC BRAKES ON VEHICLE DECELERATION

Bojana Bošković[1], Nadica Stojanović[2], Ivan Grujić[3], Saša Babić[4], Branimir Milosavljević[5]

ABSTRACT: Braking system is one part of the equation that leads to the desired deceleration of the vehicle. Vehicle dynamics are equally important and should be optimized to achieve maximum deceleration of the vehicle. Whether the driver brakes and stops the vehicle in an emergency, it must be able to stop safely. This means that he does not harm himself or other traffic participants. Velocity makes braking more difficult because higher velocities require higher braking forces. When they are moving at high velocities, more braking force is needed to slow them down. High braking forces lead to high deceleration values. When high braking force is applied, the vehicle will decelerate very quickly, however, high decelerations affect the brakes. In order to slow down the vehicle, a very large braking force is applied, and the work performed will lead to a large amount of thermal energy in the brakes, which can cause them to overheat and thus endanger traffic safety. The paper will define the influence of disc brake thermal stress on vehicle deceleration for different initial velocities

KEY WORDS: *deceleration, braking, thermal stress, traffic safety*

[1] *Bojana Bošković, Academy of professional studies Šumadija, Department in Trstenik, Radoja Krstića 19, 37240 Trstenik, Serbia, bboskovic@asss.edu.rs, https://orcid.org/0000-0001-8622-9874, (*Corresponding author)*

2 Nadica Stojanović, Faculty of Engineering, University of Kragujevac, 6 Sestre Janjić Str., 34000 Kragujevac, Serbia, nadica.stojanovic@kg.ac.rs, https://orcid.org/0000-0002-4199-0587

3 Ivan Grujić, Faculty of Engineering, University of Kragujevac, 6 Sestre Janjić Str., 34000 Kragujevac, Serbia, ivan.grujic@kg.ac.rs, https://orcid.org/0000-0003-0572-1205

4 Saša Babić, Academy of professional studies Šumadija, Department in Trstenik, Radoja Krstića 19, 37240 Trstenik, Serbia, sbabic@asss.edu.rs, -

5 Branimir Milosavljević, Academy of professional studies Šumadija, Department in Trstenik, Radoja Krstića 19, 37240 Trstenik, Serbia, bmilosavljevic@asss.edu.rs, -

UTICAJ TERMIČKOG NAPREZANJA DISK KOČNICA NA USPORAVANJE VOZILA

REZIME: Kočioni sistem je deo jednačine koji dovodi do željenog usporavanja vozila. Dinamika vozila je podjednako važna i treba je optimizovati da bi se postiglo maksimalno usporavanje vozila. Bez obzira da li vozač koči i zaustavlja vozilo u slučaju nužde, ono mora biti u stanju da se bezbedno zaustavi. To znači da ne šteti sebi niti drugim učesnicima u saobraćaju. Brzina otežava kočenje jer veće brzine zahtevaju veće sile kočenja. Kada se kreću velikim brzinama, potrebna je veća sila kočenja da bi se usporile. Velike sile kočenja dovode do visokih vrednosti usporavanja. Kada se primeni velika sila kočenja, vozilo će usporiti veoma brzo, međutim, velika usporavanja utiču na kočnice. Da bi se vozilo usporilo, primenjuje se veoma velika sila kočenja, a izvršeni rad će dovesti do velike količine toplotne energije u kočnicama, što može izazvati njihovo pregrevanje i time ugroziti bezbednost saobraćaja. U radu će biti definisan uticaj termičkog naprezanja disk kočnice na usporavanje vozila za različite početne brzine

KLJUČNE REČI: *usporavanje, kočenje, termički stres, bezbednost saobraćaja*

THE MODERN APPROACH TO PROBLEM-SOLVING IN MECHANICAL ENGINEERING - APPLICATION OF ARTIFICIAL INTELLIGENCE

Bojana Bošković, Nadica Stojanović, Ivan Grujić, Saša Babić, Branimir Milosavljević

INTRODUCTION

The first cars were equipped with simple braking mechanisms that were far from efficient and posed significant safety risks. The first disc brakes were patented by Frederick William Lanchester in 1902. The first modern disc brake system was introduced in the production Studebaker Avanti in 1962, which had Bendix disc brakes on all four wheels. The reason this system was so successful was that it used a vacuum booster to reduce the force the driver has to apply to the pedal/shoe during the braking process.

The history of brake technology shows how far it has come, in terms of safety and performance. From a simple rope-operated brake to an advanced electronic braking system, brakes have come a long way over the past hundred years. All this is aimed at improving the state of traffic safety.

The brake system from the aspect of the technical correctness of the vehicle is a system that directly affects the safety of vehicle participation in traffic. The role of the braking system is to slow down and/or stop the vehicle, that is, to adapt to traffic conditions, all in order to prevent a traffic accident. In addition, the role of the brake system is to prevent the vehicle from moving when the vehicle is parked, i.e. to keep it stationary.

The aim of this paper is to define the influence of disc brake thermal stress on vehicle deceleration for different initial velocities, in order to improve traffic safety.

1   VEHICLE DECELERATION

At the beginning of the 16th century, the Italian scientist Galileo Galilei was the first to deal with the concept of acceleration. By studying moving objects, he came to the conclusion that acceleration is exactly a change in velocity over a certain period of time. However, the physicist Isaac Newton just expanded Galileo's discoveries and wrote about it in his book *Philosophiæ Naturalis Principia Mathematica* or just *Principia* [8]. All Newton's laws are defined in this book, which also includes Newton's Second Law, which refers to acceleration and reads: The acceleration of an object depends on the mass of the object and the amount of force applied, Equation 1. Newton's laws played a key role in defining and disseminating acceleration.

$$F = m \cdot a,\qquad\qquad\qquad(1)$$

where:

m – body mass, and

a – acceleration.

The value of deceleration during intensive braking is one of the important input data for traffic accident analysis [5]. In physics, deceleration (negative acceleration) represents a decrease in velocity per time. Deceleration is a vector quantity that can be obtained by taking the first derivative of velocity (also a vector quantity) with respect to time, Equation 2.

$$\overrightarrow{j(t)} = \frac{\overrightarrow{dV}}{dt} \ , \tag{2}$$

where:

$\overrightarrow{j(t)}$ – deceleration (negative acceleration), $d\vec{V}$ – reduction of velocity, and dt – time interval.

The velocity of vehicle participating in a traffic accident, during expertise, is often determined in accordance with the length of traces of braking from tires. In this case, the values of vehicle's velocity are used for calculations, which are selected from the relevant references. Experimental research in such situations where it is necessary to determine the braking parameters of vehicle that participated in the traffic accident are not implemented enough. Therefore, it is of great importance to calculate the velocity of the vehicle in accordance with the defined deceleration values on the basis of which the vehicles limit velocities.

The braking system is one of the most complex systems on the vehicle. Its basic function is to reduce the velocity of the vehicle, as well as to stop the vehicle in a timely manner. The vehicle must ensure that the slowdown is such not to disturb the stability of the vehicle, i.e. the comfort of passengers. Maintenance of the balance between these requirements is challenging. In the last thirty years, numerous researches were conducted to give answers to the question: "What affects the braking process the most?".

In the braking process, it is necessary to achieve the force of braking corresponding to the kinetic energy of the vehicle. There are two types of braking: free and intense/forced braking. The difference between intense and free braking is that in intense braking is achieved almost immediately, so it can be considered constant, while in free braking it takes place through three characteristic phases. The first phase represents a rise of deceleration to maximum value, in the second phase there is a stabilization of deceleration that can now be considered as full deceleration, while in the third phase, deceleration decreases to zero.

The braking process is achieved by friction between brake disc and brake pads. During the friction process, the surface is heated in contact which significantly reduces braking efficiency. The reduction of braking efficiency further leads to reducing the value of deceleration, which causes longer braking distance. This is a huge problem for traffic safety.

2   THE INFLUENCE OF VARIOUS PARAMETERS ON THE DECELERATION

For intersection design, deceleration lane design, traffic simulation modelling, vehicular emission and fuel consumption modelling, etc. deceleration characteristics of vehicles are important. Maximum deceleration rate generally increases with increase in maximum velocity of all vehicle types. Authors [7] conducted that car employ highest deceleration rates while truck use the lowest among the vehicle types.

Vehicles with higher maximum velocity have higher deceleration time, deceleration distance, and lower deceleration rates. At deceleration manoeuver, vehicles with high velocity needs more time to stop compared to one with low velocity [9]. The critical velocity (at which driver attains maximum deceleration) changes with vehicle type and increases with approach velocity. This indicates that at higher approach velocity, the drivers achieve their maximum deceleration rate quickly to stop at the earliest [4].

While braking, most of the kinetic energy are converted into thermal energy and increase the disc temperature [3]. This is very dangerous because overheating may result in brake system

breakdown. Through the brake disc the temperature stability is achieved [2]. The highest thermal loads happen during rescue braking near the start of the deceleration phase [1].

Kudarauskas [6] conducted an experiment and concluded that the settled deceleration of vehicles with ABS varied from 8.00 m/s^2 (when the velocity was 40 km/h), then 8.41 m/s^2 (upon 60 km/h) up to 8.76 m/s^2 (upon 80 km/h), and the maximum values often were over 9 m/s^2. In vehicles without ABS, deceleration varied from 7.00 m/s^2 (upon 40 km/h), 6.89 m/s^2 (upon 60 km/h) up to 6.66 m/s^2 (upon 80 km/h), and the maximum values often were up to 8.3 m/s^2. On increase of initial velocity, the difference of deceleration in vehicles with and without ABS increased as well and was equal (for different velocities) to 11.5%, 18.1% and 24%, respectively.

Stojanovic et al. [10] conducted two experimental tests for the same vehicle type for different velocities (60 km/h and 80 km/h) were the other parameters: initial temperature, the mass of the simulated vehicle, number of repetitions) were the same for both tests. The authors came to the conclusion that an increase in initial velocity causes a longer braking distance as well as a higher disc temperature.

3 EXPERIMENTAL INVESTIGATION OF THE INFLUENCE OF TEMPERATURE ON DECELERATION FOR DIFFERENT INITIAL VELOCITIES

The test rig for the experimental investigation of disk brakes thermal stresses is BRAKE DYNO 2020 and its scheme is shown in Figure 1.
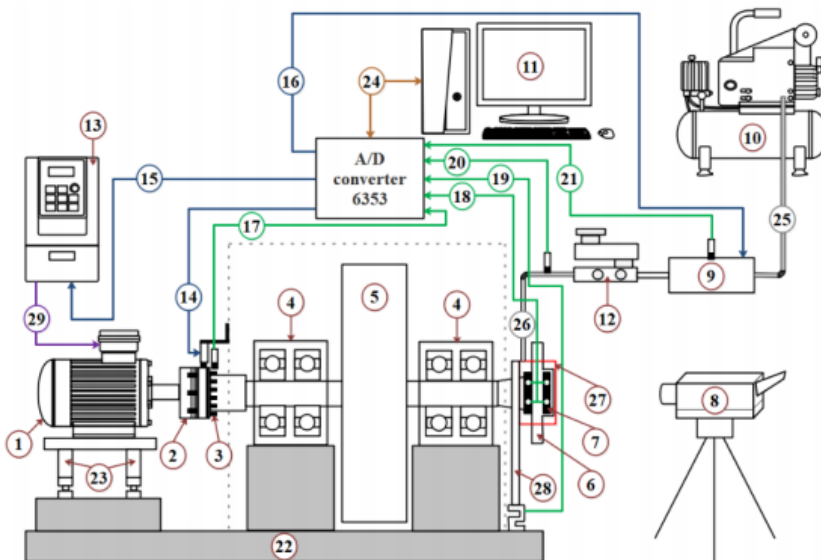

Figure 1 The scheme of the test rig

An experimental investigation was carried out with the aim of determining how the vehicle velocity affects the value of the temperature of the disc brake, how it is further reflected in the value of the deceleration and braking distance. Before starting the measurement, the test conditions were defined, Figure 2. The test rig simulates a quarter of the vehicle's mass,

which for each initial velocity value was 300 kg. The pressure in the brake installation was the same for all measurements – 5 MPa. The initial velocities were varied and were 60 km/h, 70 km/h, 80 km/h, 90 km/h and 100 km/h, respectively.

Based on the obtained data on the drop in speed over time, the actual value of the deceleration was obtained. The braking distance is calculated as the integral of the speed in a certain time interval:

$$S = \int_{t_0}^{t_1} V(t)\,dt \tag{3}$$

Where:

t_0 – time at the beginning of the braking process (it is usually taken to be $t_0 = 0$), and

t_1 – time required to stop the vehicle.
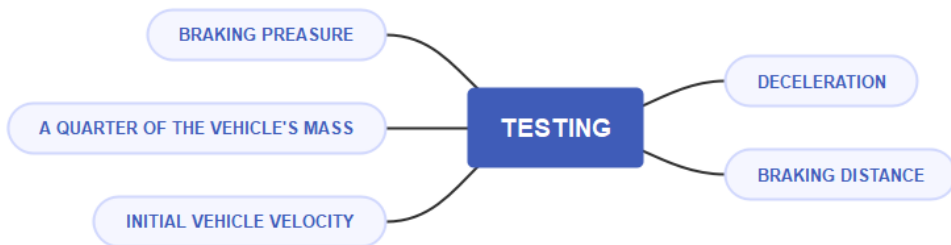
Figure 2 Experimental procedure

The input parameters are set on the test rig. After that, the desired initial velocity is achieved. After reaching the desired initial velocity, the brake is activated for the desired vehicle. During the braking process from the desired initial velocity to complete stopping, simulating intense braking, and the velocity drop is monitored. All obtained data for each measurement is stored on the computer memory. The last step is the processing and analysis of the obtained data, and certain conclusions are drawn based on the obtained analysis.

4   RESULTS AND DISCUSSION

Five measurements were taken and all measurements were with the same initial conditions (a quarter of the vehicle's mass was 300 kg, and the pressure in the brake installation was 5 MPa).

During the braking process, at an initial velocity of 60 km/h, the temperature of the brake pad was 32.1 °C. The maximum deceleration value was 8.44 m/s^2, while the braking distance was 21.7 m, Figure 3.
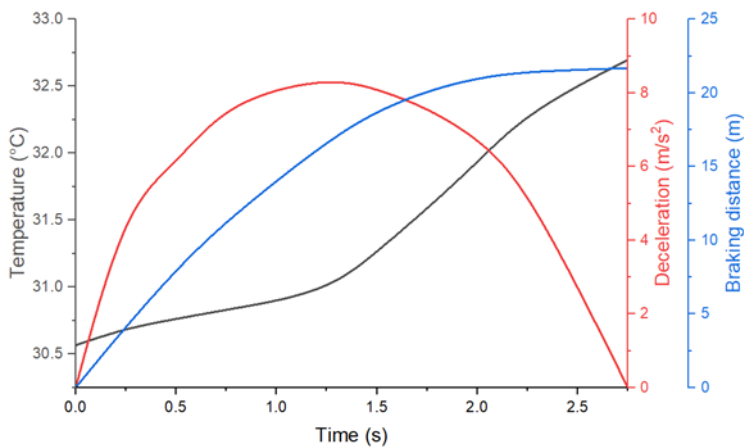
Figure 3 Dependence of deceleration and braking distance on temperature for initial velocity 60 km/h

In a repeated experiment, the value of the initial velocity was changed. When the initial velocity was 70 km/h, the maximum temperature measured on the brake pad was 36.2 °C. The maximum deceleration value measured is 10.9 m/s^2. The braking distance for initial velocity of 70 km/h was 28.2 m, as shown in Figure 4.
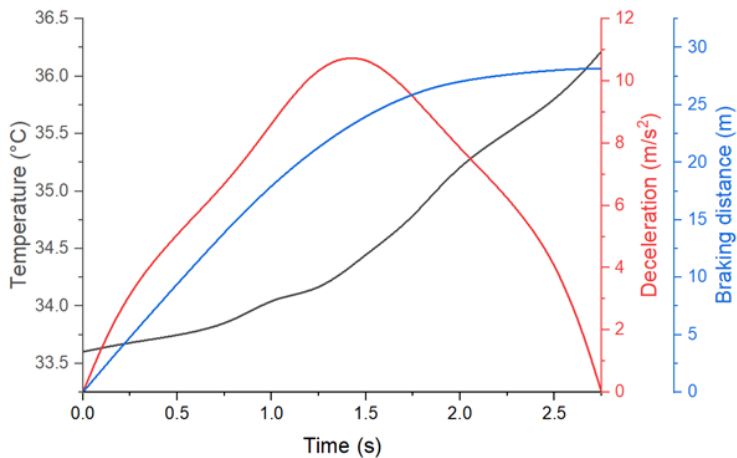

Figure 4 Dependence of deceleration and braking distance on temperature for velocity 70 km/h

The third measurement, Figure 5, that was carried out and had the same initial conditions as the previous two measurements, with the fact that in the third measurement the initial velocity was 80 km/h. Maximum measured temperature was 39 °C, the maximum recorded deceleration value was 9.8 m/s^2, while the braking distance was 39.2 m.
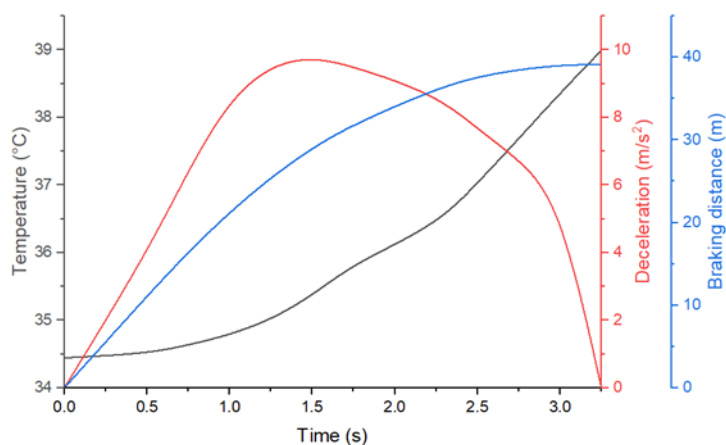
Figure 5 Dependence of deceleration and braking distance on temperature for initial velocity 80 km/h

In the fourth measurement, the initial velocity was 90 km/h, Figure 6. All other conditions were as in previous measurements. The temperature measured on the brake pad was 44.9 °C, the maximum deceleration measured was 11 m/s^2, and the braking distance was 44.6 m.
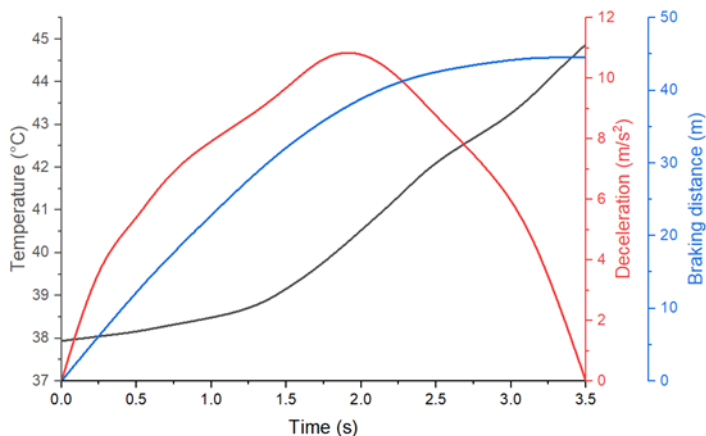

Figure 6 Dependence of deceleration and braking distance on temperature for initial velocity 90 km/h

In the last measurement, at an initial velocity of 100 km/h, the maximum measured temperature was 44.9 °C, as well as in the previous measurement at a velocity of 90 km/h. The maximum deceleration value was 10.9 m/s^2, and the braking distance was 61.2 m, as shown in Figure 7.
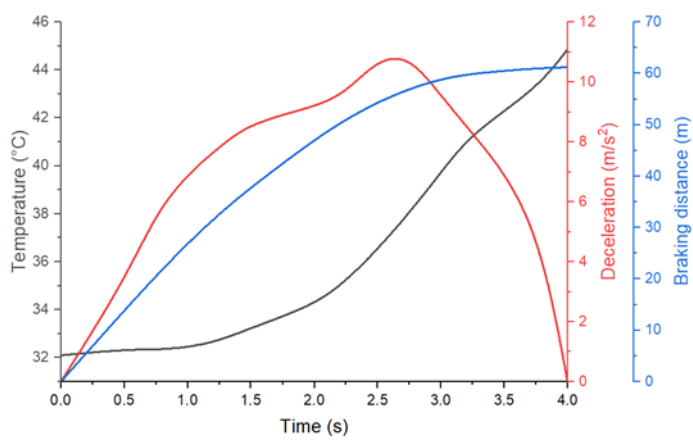
Figure 7 Dependence of deceleration and braking distance on temperature for initial velocity 100 km/h

It can be concluded that with the increment of initial velocity, there was an increase in temperature, as well as an increase in the braking distance, which tripled. However, the trend of change in deceleration is different. The highest value of deceleration was recorded at velocities 70 km/h, 90 km/h and 100 km/h, and the lowest at a velocity of 60 km/h, shown in Figure 8.
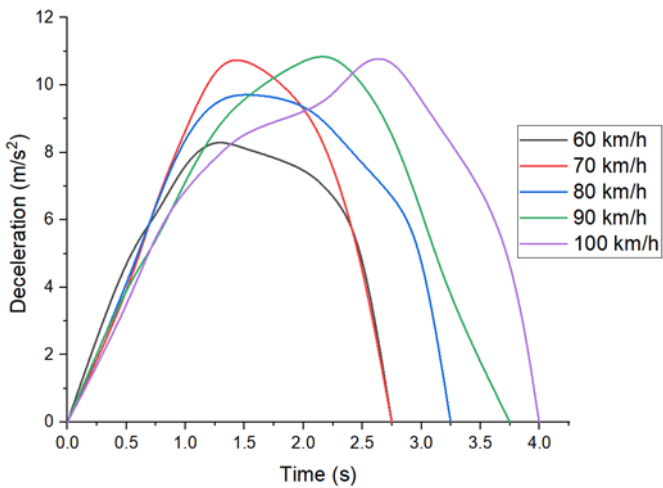

Figure 8 Deceleration for different initial velocities

The deceleration values obtained on the test bench differ from the ideal deceleration values because they do not take into consideration the deceleration of the whole vehicle, but the deceleration of the disc brake. Floating calliper is the reason for the appearance of peaks.

The obtained deceleration values differ from those shown in the paper [7], because the authors considered decelerations for different categories of vehicles, and therefore the masses of those vehicles differ from the mass used in this research.

5   CONCLUSION

The mass of the vehicle, the pressure in the brake installation, as well as the initial velocity have a great influence on the braking process. The research carried out led to the conclusion that the braking temperature increases as the velocity increases in passenger vehicles, as does the braking distance. The deceleration is the smallest for the velocity of 60 km/h, and almost approximately for the initial velocities of 70 km/h, 90 km/h and 100 km/h.

Further research should be directed at investigating how repeated braking, characteristic for stop-and-go driving, affects deceleration and braking distance.

REFERENCES

[1]   Adamowicz, A., Grzes, P.: "Analysis of disc brake temperature distribution during single braking under non-axisymmetric load", Applied Thermal Engineering, Vol. 31, 2011, pp. 1003-1012,

[2]   Agrawal, K., Patil, L.N., Chavan, K.V., Nimbalkar U.D.: "A computational analysis of heat transfer in solid and vented disc brakes: CFD simulation and thermal performance assessment", Multiscale and Multidisciplinary Modeling, Experiments and Design, 2024,

[3]   Akop, M.Z., Kien, R., Mansor, M.R., Mohd Rosli, M.A.: "Thermal stress analysis of heavy truck brake disc rotor", Journal of Mechanical Engineering and Technology, Vol. 1, No. 1, 2009, pp. 43-52,

[4]   Bokare, P.S., Maurya, A.K.: "Acceleration-deceleration behaviour of various vehicle types", Transportation Research Procedia, Vol. 25, 2017, pp. 4733-4749,

[5]   Kolla, E., Ondruš, J., Gogola, M., Šarić, Ž.: "Braking characteristics of the specified modern electric vehicle during intensive braking", Advances in Science and Technology Research Journal, Vol. 14, No. 3, 2020, pp. 125-34,

[6]   Kudarauskas, N.: "Analysis of emergency braking of a vehicle", Transport, Vol. 22, No. 3, 2007, pp.154-159,

[7]   Maurya, A.K., Bokare, P.S.: "Study of deceleration behaviour of different vehicle types", International Journal for Traffic and Transport Engineering, Vol. 2, No. 3, 2012, pp. 253-270,

[8]   Newton, I.: "Philosophiæ naturalis principia mathematica", Londini: Apud G. & J. Innys, 1726,

[9]   Omar, N., Prasetijo, J., Daniel, B.D., Abdullah, M.A.E., Ismail, I.: "Study of car acceleration and deceleration characteristics at dangerous route FT050", 4th International Conference on Civil and Environmental Engineering for Sustainability (IConCEES 2017), 4–5 December 2017, Langkawi, Malaysia, pp. 1-6,

[10]   Stojanovic, N., Grujic, I., Abdullah, O.I., Belhocine, A., Glisovic, J.: "The determination of the disc brake thermal stresses for different vehicle speeds", 9th International Congress Motor Vehicles & Motors 2022, Kragujevac, 2022, pp. 1-8.

NOTIFICATION TO AUTHORS

The Journal MVM publishes original papers which have not been previously published in other journals. This is responsibility of the author. The authors agree that the copyright for their article is transferred to the publisher when the article is accepted for publication.

The language of the Journal is English.

Journal *Mobility & Vehicles Mechanics* is at the SSCI list.

All submitted manuscripts will be reviewed. Entire correspondence will be performed with the first-named author.

Authors will be notified of acceptance of their manuscripts, if their manuscripts are adopted.

INSTRUCTIONS TO AUTHORS AS REGARDS THE TECHNICAL ARRANGEMENTS OF MANUSCRIPTS:

Abstract is a separate Word document, "*First author family name_ABSTRACT.doc*". Native authors should write the abstract in both languages (Serbian and English). The abstracts of foreign authors will be translated in Serbian.

This document should include the following: 1) author's name, affiliation and title, the first named author's address and e-mail – for correspondence, 2) working title of the paper, 3) abstract containing no more then 100 words, 4) abstract containing no more than 5 key words.

The manuscript is the separate file, „*First author family name_Paper.doc*" which includes appendices and figures involved within the text. At the end of the paper, a reference list and eventual acknowledgements should be given. References to published literature should be quoted in the text brackets and grouped together at the end of the paper in numerical order.

Paper size: Max 16 pages of B5 format, excluding abstract
Text processor: Microsoft Word
Margins: left/right: mirror margin, inside: 2.5 cm, outside: 2 cm, top: 2.5 cm, bottom: 2 cm
Font: Times New Roman, 10 pt
Paper title: Uppercase, bold, 11 pt
Chapter title: Uppercase, bold, 10 pt
Subchapter title: Lowercase, bold, 10 pt
Table and chart width: max 125 mm
Figure and table title: Figure _ (Table _): Times New Roman, italic 10 pt

Manuscript submission: application should be sent to the following e-mail:

mvm@kg.ac.rs ; lukicj@kg.ac.rs
or posted to address of the Journal:
University of Kragujevac – Faculty of Engineering
International Journal M V M
Sestre Janjić 6, 34000 Kragujevac, Serbia

The Journal editorial board will send to the first-named author a copy of the Journal offprint.

OBAVEŠTENJE AUTORIMA

Časopis MVM objavljuje orginalne radove koji nisu prethodno objavljivani u drugim časopisima, što je odgovornost autora. Za rad koji je prihvaćen za štampu, prava umnožavanja pripadaju izdavaču.

Časopis se izdaje na engleskom jeziku.

Časopis *Mobility & Vehicles Mechanics* se nalazi na SSCI listi.

Svi prispeli radovi se recenziraju. Sva komunikacija se obavlja sa prvim autorom.

UPUTSTVO AUTORIMA ZA TEHNIČKU PRIPREMU RADOVA

Rezime je poseban Word dokument, "*First author family name_ABSTRACT.doc*". Za domaće autore je dvojezičan (srpski i engleski). Inostranim autorima rezime se prevodi na srpski jezik. Ovaj dokument treba da sadrži: 1) ime autora, zanimanje i zvanje, adresu prvog autora preko koje se obavlja sva potrebna korespondencija; 2) naslov rada; 3) kratak sažetak, do 100 reči, 4) do 5 ključnih reči.

Rad je poseban fajl, „*First author family name_Paper.doc*" koji sadrži priloge i slike uključene u tekst. Na kraju rada nalazi se spisak literature i eventualno zahvalnost. Numeraciju korišćenih referenci treba navesti u srednjim zagradima i grupisati ih na kraju rada po rastućem redosledu.

Dužina rada: Najviše 16 stranica B5 formata, ne uključujući rezime
Tekst procesor: Microsoft Word
Margine: levo/desno: mirror margine; unurašnja: 2.5 cm; spoljna: 2 cm, gore: 2.5 cm, dole: 2 cm
Font: Times New Roman, 10 pt
Naslov rada: Velika slova, bold, 11 pt
Naslov poglavlja: Velika slova, bold, 10 pt
Naslov potpoglavlja: Mala slova, bold, 10 pt
Širina tabela,dijagrama: max 125 mm
Nazivi slika, tabela: Figure __ (Table _): Times New Roman, italic 10 pt

Dostavljanje rada elektronski na E-mail: **mvm@kg.ac.rs ; lukicj@kg.ac.rs**

ili poštom na adresu Časopisa
Redakcija časopisa M V M
Fakultet inženjerskih nauka
Sestre Janjić 6, 34000 Kragujevac, Srbija

Po objavljivanju rada, Redakcija časopisa šalje prvom autoru jedan primerak časopisa.